

EFFECTIVE BEHAVIOR OF SOLITARY WAVES OVER RANDOM TOPOGRAPHY*

JOSSELIN GARNIER[†], JUAN CARLOS MUÑOZ GRAJALES[‡], AND ANDRÉ NACHBIN[§]

Abstract. The deformation of a nonlinear pulse traveling in a dispersive random medium can be studied with asymptotic analysis based on separation of scales when the propagation distance is large compared to the correlation length of the random medium. We consider shallow water waves with a spatially random depth. We use a formulation in terms of a terrain-following Boussinesq system. We compute the effective evolution equation for the front pulse which can be written as a dissipative Kortweg-de Vries equation. We study the soliton dynamics driven by this system. We show, both theoretically and numerically, that a solitary wave is more robust than a linear wave in the early steps of the propagation. However, it eventually decays much faster after a critical distance corresponding to the loss of about half of its initial amplitude. We also perform an asymptotic analysis for a class of random bottom topographies. A universal behavior is captured through the asymptotic analysis of the metric term for the corresponding change to terrain-following coordinates. Within this class we characterize the effective height for highly disordered topographies. The probabilistic asymptotic results are illustrated by performing Monte Carlo simulations with a Schwarz–Christoffel Toolbox.

Key words. nonlinear waves, water waves, random media, solitons

AMS subject classifications. 76B15, 35R60, 35Q53

DOI. 10.1137/060676064

1. Introduction. We address the propagation of nonlinear dispersive free surface waves in a disordered one-dimensional fluid body. Regarding wave-topography interaction in a homogeneous medium, three characteristic length scales are important in studying different regimes of propagation: the typical depth h_0 , the typical wavelength λ_0 , and the typical amplitude of the wave elevation a_0 . We consider the framework corresponding to shallow water waves where $a_0 \ll h_0 \ll \lambda$, so that the problem can be written as a weakly dispersive, weakly nonlinear system. In this paper the lower boundary is a disordered surface modeled by a stationary random process. Two new length scales appear: the horizontal length scale, defined as the correlation length of the random fluctuations of the bottom, is denoted by l_c , while the typical amplitude of the random fluctuations is denoted by δh . We shall study this problem in two different asymptotic regimes. We assume either that the amplitude of the fluctuations of the bottom is small compared to the average depth $\delta h \ll h_0$, or that the typical amplitude is of the same order as the average depth $\delta h \sim h_0$, but the correlation length is much smaller than the typical wavelength $l_c \ll \lambda$. We also assume that the propagation distance is large. We carry out an asymptotic analysis based on these assumptions. Our goal is to derive an effective evolution equation governing

*Received by the editors November 27, 2006; accepted for publication (in revised form) August 27, 2007; published electronically December 19, 2007.

<http://www.siam.org/journals/mms/6-3/67606.html>

[†]Laboratoire de Probabilités et Modèles Aléatoires & Laboratoire Jacques-Louis Lions, Université Paris 7, 2 Place Jussieu, 75251 Paris Cedex 05, France (garnier@math.jussieu.fr). This author's research was supported by ANR.

[‡]Departamento de Matemáticas, Universidad del Valle, A.A. 25360 Cali, Colombia (jcarlmz@yahoo.com). This author's research was supported by COLCIENCIAS under grant 1106 05 16858.

[§]Instituto de Matemática Pura e Aplicada, Est. D Castorina 110, Jardim Botânico, Rio de Janeiro, RJ 22460-320, Brazil (nachbin@impa.br). This author's research was supported by CNPq/Brazil under grant 300368/96-8.

the propagation of the free surface wave. This is done by applying an asymptotic stochastic analysis to the Lagrangian formulation of the problem, following the strategy that we introduced in [12] in a weakly heterogeneous regime for a nonlinear hyperbolic system. Here we start with a one-dimensional, shallow water Boussinesq system which is transformed into a Lagrangian frame by using the Riemann invariants of the underlying nondispersive, constant coefficient system. Applying a limit theorem for stochastic differential equations we characterize the flow along the wavefront by a viscous Kortweg–de Vries (KdV) equation. Actually the diffusive-like term is more complicated than an effective viscosity and has the form of a pseudodifferential operator, but it reduces to such a term when the correlation length of the medium is much smaller than the pulse width.

We give a brief background on the mathematical theory that has been developed and which is along the lines of our study. We use a mathematical formulation that has been successfully used by the authors in other nonlinear settings, namely a nonlinear conservation law (shallow water system) and a nonlinear advection diffusion equation (viscous shallow water model). Now we apply the technique to a different class of partial differential equations (PDEs). In what follows we use Riemann invariants in a weakly dispersive, weakly nonlinear setting for which we can consider solitary waves interacting with disorder. We shall contrast the behavior of a solitary wave with its linear counterpart. The propagation of a linear pulse through a random medium has been extensively studied [1]. In particular the O’Doherty–Anstey (ODA) theory predicts that if the pulse is observed in a Lagrangian frame that moves with a random velocity, then the pulse appears to retain its shape up to a slow spreading and attenuation [31]. A rather convincing heuristic explanation of this phenomenon is given in [5]. The mathematical treatment of this issue is addressed in [5, 6, 20, 21, 3]. An extension to dispersive water waves is provided in [11, 13, 25]. We have extended this theory to inviscid nonlinear waves in [12] and to viscous waves in [16]. It is also possible to apply a mean-field approach to water waves over a rough bottom [22, 23].

The paper is organized as follows. In section 2 we introduce the nonlinear shallow water wave model with a random depth together with the corresponding Riemann invariants. In section 3 we derive the effective viscous KdV equation governing the evolution of the front pulse in the case of a small-amplitude slowly varying topography. Section 4 is devoted to the same problem with a rapidly varying topography. In this section we also perform an asymptotic analysis for a class of rapidly varying bottom topographies. Within this class, a universal behavior is captured through the asymptotic analysis of the metric term for the corresponding change to terrain-following coordinates. In section 5 we discuss and compare the pulse attenuation and spreading in the linear regime and in the soliton regime. In section 6 we present numerical simulations to illustrate the accuracy of the theoretical predictions of the asymptotic analysis.

2. Shallow water waves with random depth.

2.1. The terrain-following Boussinesq system. The water wave problem addressed here is in a regime where Euler’s equations are valid. At the top of our domain a free surface defines the wave profile. Euler’s equations can then be recast as a potential theory problem where $(\tilde{u}, \tilde{v}) = \nabla\phi(x, y, t)$. Thus the velocity field is obtained through the velocity potential ϕ [36]. In [29] a conformal map is used to map the rough channel onto a flat strip. This is the same as changing variables from a Cartesian xy -coordinate system to an orthogonal curvilinear one, namely, in the $\xi\zeta$ -variables. This is done in such a way that at the undisturbed free surface $y \equiv 0$

and $\zeta \equiv 0$ coincide. The topography now is along a ($\zeta \equiv \text{constant}$) curve. In [29] this constant is such that ($\zeta \equiv \sqrt{\beta}$). Since we are dealing with harmonic functions (through the potential and the conformal map) it easily follows that in the curvilinear coordinates we have a new set of orthogonal velocity components $(u, v) = \nabla\phi(\xi, \zeta, t)$, where $u(\xi, \zeta, t)$ is a terrain-following component, namely, tangent to the ζ -level curves. Now the gradient is to be considered in the new set of variables. It follows [27] that a family of Boussinesq systems can be deduced, depending on the depth ζ at which the u -velocity component is evaluated. As can be seen in [27] this changes the dispersion relation in different interesting ways, through a family of Padé approximations from the original potential theory dispersion relation.

By an asymptotic analysis along the depth, the two-dimensional Euler equations can be reduced to a one-dimensional system for the wave elevation $\eta(\xi, t)$ and the terrain-following velocity component $u(\xi, \zeta, t)$, where ζ is an arbitrary fixed depth [27, 29, 36]. As our reduced model of interest, we consider the one-parameter family of Boussinesq equations that describe the evolution of surface waves in shallow channels [27]

$$(2.1) \quad M\eta_t + \left[\left(1 + \frac{\alpha\eta}{M} \right) u \right]_{\xi} - \frac{\beta}{2} \left(y_0^2 - \frac{1}{3} \right) [M\eta]_{\xi\xi t} = 0,$$

$$(2.2) \quad u_t + \eta_{\xi} + \alpha \left[\frac{u^2}{2M^2} \right]_{\xi} + \frac{\beta}{2} (y_0^2 - 1) u_{\xi\xi t} = 0,$$

where η is the wave elevation and u is the terrain-following velocity at a relative depth parameterized by y_0 [29, 27] in such a way that $y_0 = 0$ is the bottom and $y_0 = 1$ is the free surface. ξ and t are the space and time coordinates, respectively. The parameter α is the ratio of the typical wave amplitude over the mean depth. It governs the strength of the nonlinearity. The parameter β is the ratio of the squared mean depth over the squared characteristic wavelength of the wave. It governs the strength of the dispersion. These two parameters are assumed to be small. The system (2.1)–(2.2) is derived from first principles (mass and momentum conservations) in the asymptotics $\alpha \ll 1$ and $\beta \ll 1$, and it neglects terms of order $O(\alpha^2)$, $O(\alpha\beta)$, and $O(\beta^2)$. Hence, as mentioned above, the system is a weakly nonlinear, weakly dispersive asymptotic approximation of the potential theory equations for an irrotational, incompressible, and inviscid fluid. For example, this is the regime where one might have tsunamis. At early stages these waves have a few meters of height and tens of kilometers of length. Hence we are in the linear regime, and as they approach the continental shelf we enter the weakly nonlinear regime, which will account for shoaling and steepening [36]. Moreover, this long wave, of tens of kilometers or more, propagates over regions of thousands of meters and less. Hence it is clear that in this scenario $\alpha \ll 1$ and $\beta \ll 1$ are representative. Moreover, the disordered microscale features of the topography, which play a role within the framework of this paper, are those in the range of hundreds of meters to a few kilometers. A first version of this terrain-following model was given in [29], where the terrain-following velocity is depth-averaged in ζ . Then it was shown in [27] that depth-averaging u is exactly the same as using $y_0^2 = 1/3$ in the equation above. Along this frame of ideas, the model in [29] was then modified in [35], to the same order of approximation, having as a special feature the fact that the full existence and well-posedness proof could be established. A property that played a key role in the proof was that for $y_0^2 = 2/3$ an energy-type integral could be found. Here, for a different reason, the same parameter value will play an important role.

The variable coefficient $M(\xi)$ is a smooth orography-dependent function which

appears as a consequence of a change of variables from Cartesian to curvilinear coordinates. $M(\xi)$ is the leading-order term of the Jacobian of the transform, and it is deduced from the physical orography $y = h(x)$ which describes the channel's depth, whose averaged value has been normalized to 1. The topography profile $h(x) = 1 + n(x)$ can be rapidly varying, discontinuous, or even multivalued, and no mild slope condition is required. The only requirement is that there exists a constant $C \in (0, 1)$ such that $\|n\|_\infty \leq C$. In the terrain-following system the physical orography $h(x) = 1 + n(x)$ is replaced by the metric coefficient

$$(2.3) \quad M(\xi) = 1 + \frac{\pi}{4\sqrt{\beta}} \int_{-\infty}^{\infty} \frac{n(x(\xi_0, -\sqrt{\beta}))}{\cosh^2 \left[\frac{\pi}{2\sqrt{\beta}}(\xi_0 - \xi) \right]} d\xi_0,$$

where $(x, y) \mapsto (\xi, \zeta)$ is the coordinate transform used for the conformal mapping in the derivation of the system [29]. Note that the amplitude of M can be of order 1 and it is a C^∞ -function by the convolution with the sech^2 function.

In this paper we shall model the random topography $n(x)$ as the realization of a stationary random process. This in turn implies that M is a smooth random process. The random process n that describes the fluctuations of the bottom is assumed to be bounded by a deterministic constant less than 1 and to have strong mixing properties. The autocorrelation function

$$(2.4) \quad \gamma(x) = \mathbb{E}[n(y)n(y+x)]$$

is assumed to decay fast enough so that it belongs to $L^{1/2}$; i.e., γ decays at infinity fast enough to ensure the convergence of the integral $\int_{-\infty}^{\infty} |\gamma(x)|^{1/2} dx$. We define the correlation length of the medium as

$$(2.5) \quad l_c = \frac{\int_{-\infty}^{\infty} |\gamma(x)| dx}{\gamma(0)}.$$

It represents the typical variation length scale of the random topography.

2.2. The Riemann invariants. We introduce the local propagation speed corresponding to the flat bottom $c = \sqrt{1 + \alpha\eta}$. We can reformulate (2.1)–(2.2) in terms of c and u to obtain

$$(2.6) \quad c_t + \frac{\alpha}{2c} \left[\left(1 + \frac{c^2 - 1}{M^2} \right) u_\xi + \left(\frac{c^2 - 1}{M^2} \right)_\xi u \right] - \frac{\beta}{2c} \left(y_0^2 - \frac{1}{3} \right) (cc_t)_{\xi\xi} = 0,$$

$$(2.7) \quad u_t + \frac{\alpha}{2} \left[\frac{u^2}{M^2} \right]_\xi + \frac{1}{\alpha} \left[\frac{c^2 - 1}{M} \right]_\xi + \frac{\beta}{2} (y_0^2 - 1) u_{\xi\xi t} = 0.$$

We define the Riemann invariants (corresponding to the unperturbed nonlinear hyperbolic system):

$$(2.8) \quad A(\xi, t) = \frac{\alpha u - 2c + 2}{\alpha}, \quad B(\xi, t) = \frac{\alpha u + 2c - 2}{\alpha}.$$

Indeed, if the dispersion parameter is vanishing $\beta = 0$ and the bottom is flat $M = 1$, then we get back the standard left- and right-going modes (A and B , respectively) of the nonlinear hyperbolic system:

$$A_t - c_- A_\xi = 0, \quad B_t + c_+ B_\xi = 0,$$

with $c_- = c - \alpha u = 1 - \alpha(3A + B)/4$ and $c_+ = c + \alpha u = 1 + \alpha(A + 3B)/4$. The identities (2.8) can be inverted:

$$u = \frac{A + B}{2}, \quad c = 1 + \alpha \frac{B - A}{4}.$$

Substituting these expressions into (2.6)–(2.7), we get the system governing the dynamics of the Riemann invariants in the presence of nonlinearity, dispersion, and randomness. If we neglect the terms of order α^2 , the Riemann invariants satisfy

$$\begin{aligned} (2.9) \quad & A_t - A_\xi + \frac{\alpha}{4}(3A + B)A_\xi - \frac{\beta}{6}A_{\xi\xi t} = \frac{\beta}{2} \left(\frac{2}{3} - y_0^2 \right) B_{\xi\xi t} \\ & + \frac{1}{2} \left(\frac{1}{M} - 1 \right) (A_\xi - B_\xi) + \frac{1}{2} \left(\frac{1}{M} \right)_\xi (A - B) \\ & + \alpha A A_\xi \left(1 - \frac{1}{M^2} \right) + \frac{\alpha}{8} \left(\frac{2}{M^2} - \frac{1}{M} - 1 \right) (A - B)(A_\xi - B_\xi) \\ & - \frac{\alpha}{16} \left(\frac{1}{M} \right)_\xi \left[(A - B)^2 + \frac{4}{M}(3A^2 + 2AB - B^2) \right], \end{aligned}$$

$$\begin{aligned} (2.10) \quad & B_t + B_\xi + \frac{\alpha}{4}(3B + A)B_\xi - \frac{\beta}{6}B_{\xi\xi t} = \frac{\beta}{2} \left(\frac{2}{3} - y_0^2 \right) A_{\xi\xi t} \\ & + \frac{1}{2} \left(\frac{1}{M} - 1 \right) (A_\xi - B_\xi) + \frac{1}{2} \left(\frac{1}{M} \right)_\xi (A - B) \\ & + \alpha B B_\xi \left(1 - \frac{1}{M^2} \right) + \frac{\alpha}{8} \left(\frac{2}{M^2} - \frac{1}{M} - 1 \right) (A - B)(A_\xi - B_\xi) \\ & - \frac{\alpha}{16} \left(\frac{1}{M} \right)_\xi \left[(A - B)^2 + \frac{4}{M}(-A^2 + 2AB + 3B^2) \right]. \end{aligned}$$

In these equations we have neglected terms of order $O(\alpha^2)$, consistently with the derivation of the system (2.1)–(2.2), but we have kept all terms depending on M . In the absence of random perturbations, that is, if $M = 1$, these equations can be reduced to

$$(2.11) \quad A_t - A_\xi + \frac{\alpha}{4}(3A + B)A_\xi - \frac{\beta}{6}A_{\xi\xi\xi} = \frac{\beta}{2} \left(\frac{2}{3} - y_0^2 \right) B_{\xi\xi t},$$

$$(2.12) \quad B_t + B_\xi + \frac{\alpha}{4}(3B + A)B_\xi + \frac{\beta}{6}B_{\xi\xi\xi} = \frac{\beta}{2} \left(\frac{2}{3} - y_0^2 \right) A_{\xi\xi t}.$$

By choosing $y_0^2 = 2/3$, the right-hand sides vanish, and we get that the system supports pure left- and right-going waves satisfying a KdV equation. From now on we adopt this choice for y_0 . Recall that this is the special value that enables the existence and well-posedness proof given in [35].

In the following sections, we consider the system (2.9)–(2.10) in the presence of a random topography in the right half-space, while the medium is unperturbed in the left half-space. The system is completed by the initial condition corresponding to a right-going wave incoming from the homogeneous left half-space

$$(2.13) \quad A(\xi, t) = 0, \quad B(\xi, t) = f(t - \xi), \quad t < 0,$$

where the function f is compactly supported in $(0, \infty)$.

2.3. The linear hyperbolic approximation. If we neglect terms of order α and β , that is, if we neglect all nonlinear and dispersive contributions, then the system for the Riemann invariants can be reduced to

$$\frac{1}{2} \begin{pmatrix} 1 + \frac{1}{M} & 1 - \frac{1}{M} \\ -1 + \frac{1}{M} & -1 - \frac{1}{M} \end{pmatrix} \frac{\partial}{\partial \xi} \begin{pmatrix} A \\ B \end{pmatrix} = \frac{\partial}{\partial t} \begin{pmatrix} A \\ B \end{pmatrix} + \frac{1}{2} \left(\frac{1}{M} \right)_\xi \begin{pmatrix} -1 & 1 \\ -1 & 1 \end{pmatrix} \begin{pmatrix} A \\ B \end{pmatrix}.$$

The matrix in front of the partial ξ -derivative can be inverted, which gives

$$(2.14) \quad \frac{\partial}{\partial \xi} \begin{pmatrix} A \\ B \end{pmatrix} = Q \frac{\partial}{\partial t} \begin{pmatrix} A \\ B \end{pmatrix} + \frac{1}{2} \frac{M_\xi}{M} \begin{pmatrix} 1 & -1 \\ -1 & 1 \end{pmatrix} \begin{pmatrix} A \\ B \end{pmatrix},$$

where

$$(2.15) \quad Q(\xi) = \frac{1}{2} \begin{pmatrix} M(\xi) + 1 & M(\xi) - 1 \\ 1 - M(\xi) & -M(\xi) - 1 \end{pmatrix}.$$

The identity (2.14), which holds true up to terms of order $O(\alpha)$, $O(\beta)$, will be used in the forthcoming sections to rewrite the system (2.9)–(2.10) for the Riemann invariants as a PDE of the form

$$\frac{\partial}{\partial \xi} \begin{pmatrix} A \\ B \end{pmatrix} = F(A, B, A_t, B_t, A_{tt}, B_{tt}, A_{ttt}, B_{ttt}, M, M_\xi, M_{\xi\xi}),$$

with the same accuracy as the original system, that is, up to terms of order $O(\alpha^2)$, $O(\beta^2)$, and $O(\alpha\beta)$.

In the linear hyperbolic approximation, (2.14) can be processed directly to study the wave dynamics. Indeed, the matrix Q can be diagonalized. The eigenvalues of the matrix $Q(\xi)$ are $\pm M^{1/2}(\xi)$. We introduce the matrix U defined by

$$(2.16) \quad U(\xi) = \frac{1}{2} \begin{pmatrix} M^{1/4}(\xi) + M^{-1/4}(\xi) & -M^{1/4}(\xi) + M^{-1/4}(\xi) \\ -M^{1/4}(\xi) + M^{-1/4}(\xi) & M^{1/4}(\xi) + M^{-1/4}(\xi) \end{pmatrix},$$

which is such that

$$U^{-1}(\xi)Q(\xi)U(\xi) = M^{1/2}(\xi) \begin{pmatrix} 1 & 0 \\ 0 & -1 \end{pmatrix}.$$

In terms of the new variables

$$\begin{pmatrix} A_1 \\ B_1 \end{pmatrix}(\xi, t) = U^{-1}(\xi) \begin{pmatrix} A \\ B \end{pmatrix}(\xi, t) \frac{1}{M^{1/2}(\xi)},$$

(2.14) has the simple form

$$(2.17) \quad \frac{\partial}{\partial \xi} \begin{pmatrix} A_1 \\ B_1 \end{pmatrix} = M^{1/2} \begin{pmatrix} 1 & 0 \\ 0 & -1 \end{pmatrix} \frac{\partial}{\partial t} \begin{pmatrix} A_1 \\ B_1 \end{pmatrix} - \frac{1}{4} \frac{M_\xi}{M} \begin{pmatrix} 0 & 1 \\ 1 & 0 \end{pmatrix} \begin{pmatrix} A_1 \\ B_1 \end{pmatrix}.$$

This equation clearly exhibits the two relevant phenomena in linear random medium. The first term in the right-hand side describes a change of the velocity described by $M^{1/2}$. The second term in the right-hand side describes a coupling between the two modes imposed by the term M_ξ/M , which is the reflectivity coefficient as in [3].

3. Small-amplitude, slowly varying topography. We consider the weakly nonlinear, weakly dispersive system (2.9)–(2.10). We introduce a small dimensionless parameter $\varepsilon > 0$ so that the small nonlinear and dispersion parameters can be written as

$$(3.1) \quad \alpha = \varepsilon^2 \alpha_0, \quad \beta = \varepsilon^2 \beta_0.$$

Here α_0 (resp., β_0) is the normalized nonlinearity (resp., dispersion) parameter which is a nonnegative number of order 1. In this section we also assume that the random topography has *small-amplitude fluctuations* and is *slowly varying*, in the sense that its correlation length is of the same order as the typical wavelength of the incoming wave. It turns out that the suitable scaling that gives rise to a nontrivial asymptotic regime consists in taking

$$(3.2) \quad n(x) = \varepsilon n_0(x),$$

where n_0 is a stationary random process with standard deviation and correlation length of order one.

3.1. Smooth topography. In this section we assume that n_0 possesses derivatives and that it satisfies the moment conditions $\mathbb{E}[n_0(x_0)^2] < \infty$ and $\mathbb{E}[n_0'(x_0)^2] < \infty$. In this framework the metric coefficient $M(\xi)$ is not changed with respect to $1 + n(x)$ to leading order in ε , but there is a correction of order ε^2 described in the following lemma.

LEMMA 3.1. *The metric coefficient $M(\xi)$ can be expanded as*

$$(3.3) \quad M(\xi) = 1 + \varepsilon n_0(\xi) + \varepsilon^2 (n_1(\xi) - \gamma_0(0)) + o(\varepsilon^2),$$

where n_1 is a zero-mean random process and $\gamma_0(x) = \mathbb{E}[n_0(x_0)n_0(x_0 + x)]$ is the autocorrelation function of n_0 .

Proof. The process $M(\xi)$ is defined by (2.3). It is given by the convolution of a smooth sech^2 kernel with the composition of the random process n_0 and the real part of the conformal map $x(\xi, \zeta)$ evaluated at the unperturbed bottom $-\sqrt{\beta} = -\sqrt{\beta_0}\varepsilon$. The imaginary part $y(\xi, \zeta)$ satisfies the Laplace equation $\Delta y = 0$ in the domain $\mathbb{R} \times (-\sqrt{\beta_0}\varepsilon, 0)$ and the Dirichlet boundary conditions $y(\xi, 0) = 0$ and $y(\xi, -\varepsilon\sqrt{\beta_0}) = -\varepsilon\sqrt{\beta_0}[1 + \varepsilon n_0(x(\xi, -\varepsilon\sqrt{\beta_0}))]$. Of course, at zeroth order, we have $x = \xi$ and $y = \zeta$. By Fourier transform we can find the following representation for y :

$$y(\xi, \zeta) = \zeta + \frac{\varepsilon^2 \sqrt{\beta_0}}{2\pi} \int \frac{\sinh(k\zeta)}{\sinh(k\varepsilon\sqrt{\beta_0})} \hat{n}_1(k) e^{ik\xi} dk,$$

where $\hat{n}_1(k)$ is the Fourier transform (in ξ) of $n_0(x(\xi, -\sqrt{\beta_0}\varepsilon))$. Using the Cauchy–Riemann equation $x_\xi = y_\zeta$ gives

$$x_\xi(\xi, \zeta) = 1 + \frac{\varepsilon^2 \sqrt{\beta_0}}{2\pi} \int \frac{k \cosh(k\zeta)}{\sinh(k\varepsilon\sqrt{\beta_0})} \hat{n}_1(k) e^{ik\xi} dk.$$

Since ζ is of order ε , we can expand the \cosh and the \sinh to obtain $x_\xi(\xi, \zeta) = 1 + \varepsilon n_0(x(\xi, -\sqrt{\beta_0}\varepsilon)) + o(\varepsilon^2)$ for all $\zeta \in [-\varepsilon\sqrt{\beta_0}, 0]$. Note that if we assume that n_0 is twice differentiable, then the $o(\varepsilon^2)$ is $O(\varepsilon^3)$. Since $M(\xi) = x_\xi(\xi, 0)$ by definition [30], this gives the first corrective term of the expansion (3.3). We can also obtain a precise description of the higher-order correction. The process X^ε defined by

$$X^\varepsilon(\xi) := x\left(\frac{\xi}{\varepsilon^2}, -\sqrt{\beta_0}\varepsilon\right) - \frac{\xi}{\varepsilon^2}$$

satisfies the random ordinary differential equation (ODE)

$$\frac{dX^\varepsilon}{d\xi} = \frac{1}{\varepsilon} n_0 \left(\frac{\xi}{\varepsilon^2} + X^\varepsilon \right) + o(1).$$

By applying a diffusion-approximation theorem [32, 33], $X^\varepsilon(\xi)$ converges in distribution as $\varepsilon \rightarrow 0$ to the diffusion process $X(\xi)$ with the infinitesimal generator

$$\mathcal{L} = \int_0^\infty \mathbb{E} \left\{ n_0(x) \frac{\partial}{\partial x} \left[n_0(u+x) \frac{\partial}{\partial x} \right] \right\} du = \int_0^\infty \gamma_0(u) du \frac{\partial^2}{\partial x^2} + \int_0^\infty \gamma'_0(u) du \frac{\partial}{\partial x}$$

that can be identified as

$$X(\xi) = \sqrt{2\mu_0} W_\xi - \gamma_0(0)\xi,$$

where $\mu_0 = \int_0^\infty \gamma_0(u) du$ and W_ξ is a standard Brownian motion. This shows that the drift of X is constant and equal to $-\gamma_0(0)$, which gives the result. \square

In the forthcoming asymptotic analysis, the most important term in the expansion (3.3) is $\varepsilon n_0(\xi)$, since it is the one that is responsible for the coupling between left- and right-going modes. The contribution of the zero-mean process n_1 vanishes in the limit $\varepsilon \rightarrow 0$. The correction to the average depth

$$\mathbb{E}[M(\xi)] = 1 - \varepsilon^2 \mathbb{E}[n_0(0)^2] + o(\varepsilon^2)$$

will play a role, because it induces a change in the average velocity of order ε^2 , which gives a shift of order 1 after a propagation distance of order ε^{-2} .

Our goal is to study the wave propagation for times and distances of order ε^{-2} . Accordingly in (2.9)–(2.10) we can neglect the terms of order ε^3 . We can also use (2.14), valid up to order ε , to rewrite some ξ derivatives as time derivatives. This can be done with a sufficient accuracy for the nonlinear and dispersive terms. As a result, we obtain

$$\begin{aligned} \frac{\partial}{\partial \xi} \begin{pmatrix} A \\ B \end{pmatrix} &= Q(\xi) \frac{\partial}{\partial t} \begin{pmatrix} A \\ B \end{pmatrix} + \frac{M_\xi}{2M} \begin{pmatrix} 1 & -1 \\ -1 & 1 \end{pmatrix} \begin{pmatrix} A \\ B \end{pmatrix} \\ &+ \varepsilon^2 \frac{\alpha_0}{4} \begin{pmatrix} 3A+B & 0 \\ 0 & A+3B \end{pmatrix} \frac{\partial}{\partial t} \begin{pmatrix} A \\ B \end{pmatrix} \\ &+ \varepsilon^2 \frac{\beta_0}{6} \begin{pmatrix} -1 & 0 \\ 0 & 1 \end{pmatrix} \frac{\partial^3}{\partial t^3} \begin{pmatrix} A \\ B \end{pmatrix} + O(\varepsilon^3), \end{aligned} \tag{3.4}$$

where M_ξ is a zero-mean process of order ε and Q is given by (2.15). The first step of the derivation of the effective equation for the front pulse is based on a series of transformations to rewrite the evolution equations (3.4) of the modes by centering along the characteristic of the right-going mode. This gives an upper-triangular system that can be integrated more easily. In a second step an averaging theorem [4, 18] is applied to this system to establish an effective nonlinear equation for the front pulse for times and distances of order ε^{-2} . These computations follow the lines of the proof of the front pulse analysis in the random, nonlinear, hyperbolic case given in [12]. The result can be stated as follows.

PROPOSITION 3.2. *Let \tilde{B}_0 be the solution of the deterministic equation*

$$\frac{\partial \tilde{B}_0}{\partial \xi} = \mathcal{L} \tilde{B}_0 + \frac{3\alpha_0}{4} \tilde{B}_0 \frac{\partial \tilde{B}_0}{\partial \tau} + \frac{\beta_0}{6} \frac{\partial^3 \tilde{B}_0}{\partial \tau^3}, \tag{3.5}$$

starting from $\tilde{B}_0(0, \tau) = f(\tau)$. The front pulse $B^\varepsilon(\xi, \tau) := B(\xi/\varepsilon^2, \tau + \xi/\varepsilon^2)$, $\xi \in [0, \infty)$, $\tau \in \mathbb{R}$, converges in distribution in the space of the continuous functions (equipped with the topology associated with the supremum norm over the compact intervals) to \tilde{B} given by

$$(3.6) \quad \tilde{B}(\xi, \tau) = \tilde{B}_0(\xi, \tau - T_\xi),$$

where T_ξ is the random time shift

$$(3.7) \quad T_\xi = \frac{\sqrt{b_0(0)}}{\sqrt{2}}W_\xi + \frac{\gamma_0(0)}{2}\xi.$$

Here W_ξ is a standard Brownian motion, and the operator \mathcal{L} can be written explicitly in the Fourier domain as

$$(3.8) \quad \int_{-\infty}^{\infty} \mathcal{L}B(\tau)e^{i\omega\tau} d\tau = -\frac{b_0(2\omega)\omega^2}{4} \int_{-\infty}^{\infty} B(\tau)e^{i\omega\tau} d\tau,$$

$$(3.9) \quad b_0(\omega) = \int_0^\infty \gamma_0(x)e^{i\omega x} dx,$$

where $\gamma_0(x) = \mathbb{E}[n_0(x_0)n_0(x_0 + x)]$ is the autocorrelation function of n_0 .

The random time shift T_ξ originates from the random propagation speed. \mathcal{L} is a pseudodifferential operator that models the deterministic pulse deformation. It can be interpreted as an effective pseudoviscosity originating from the random forcing. The effective equation for the front pulse depends on randomness (through the function b_0), on dispersion (through β_0), and on nonlinearity (through α_0).

First, the pseudodifferential operator \mathcal{L} satisfies a special but rather intuitive time property. Indeed, in the time domain, we can write

$$\mathcal{L}B(\tau) = \left[\frac{1}{8}\gamma_0\left(\frac{\tau}{2}\right)\mathbf{1}_{[0,\infty)}(\tau) \right] * \left[\frac{\partial^2 B}{\partial \tau^2}(\tau) \right] = \frac{1}{8} \int_0^\infty \gamma_0\left(\frac{s}{2}\right) \frac{\partial^2 B}{\partial \tau^2}(\tau - s) ds.$$

The indicator function $\mathbf{1}_{[0,\infty)}$ is essential to interpret the convolution correctly. It means that the effective viscosity cannot diffuse the wave energy in the forward direction (ahead the front) but only in the backward direction (behind the front). This in turn implies that the reduction of the pseudodifferential operator \mathcal{L} to a second-order diffusion operator that we discuss next should be handled with precaution.

We now discuss further properties of the pseudodifferential operator \mathcal{L} . It can be divided into two parts $\mathcal{L} = \mathcal{L}_r + \mathcal{L}_i$:

$$(3.10) \quad \int_{-\infty}^{\infty} \mathcal{L}_r B(\tau)e^{i\omega\tau} d\tau = -\frac{b_r(2\omega)\omega^2}{4} \int_{-\infty}^{\infty} B(\tau)e^{i\omega\tau} d\tau,$$

$$(3.11) \quad \int_{-\infty}^{\infty} \mathcal{L}_i B(\tau)e^{i\omega\tau} d\tau = -\frac{ib_i(2\omega)\omega^2}{4} \int_{-\infty}^{\infty} B(\tau)e^{i\omega\tau} d\tau,$$

where b_r and b_i are, respectively, the real and imaginary part of b_0 :

$$b_r(\omega) = \int_0^\infty \mathbb{E}[n_0(0)n_0(x)] \cos(\omega x) dx, \quad b_i(\omega) = \int_0^\infty \mathbb{E}[n_0(0)n_0(x)] \sin(\omega x) dx.$$

By the Wiener–Khinchine theorem [24], b_r is proportional to the power spectral density of the random stationary process n_0 . As a result, b_r is nonnegative, which

shows that \mathcal{L}_r can be interpreted as an effective diffusion operator. More precisely, for small frequencies, \mathcal{L}_r behaves like a second-order diffusion. Indeed, if $\omega l_c \ll 1$, then $b_r(\omega) \simeq \mu_0$, where $\mu_0 := \int_0^\infty \gamma_0(x) dx$, and

$$\mathcal{L}_r \simeq \frac{\mu_0}{4} \frac{\partial^2}{\partial \tau^2}.$$

On the other hand, b_r decays to zero for high frequencies ω such that $\omega l_c \gg 1$. Indeed, we have assumed that $\mathbb{E}[n_0^2(0)] < \infty$, which is equal to $-\gamma_0''(0)$. By use of the inverse Fourier transform this shows that $\int \omega^2 b_r(\omega) d\omega < \infty$ and $\omega^2 b_r(\omega)$ should decay fast enough as ω goes to infinity to ensure the convergence of this integral. As a result \mathcal{L}_r has no effect on the high-frequency components.

\mathcal{L}_i is an effective dispersion operator, since it preserves the energy. It behaves like a third-order dispersion for small frequencies. Indeed, if $\omega l_c \ll 1$, then $b_i(\omega) \simeq \omega \beta_1$, where $\beta_1 := \int_0^\infty x \gamma_0(x) dx$, and

$$\mathcal{L}_i \simeq -\frac{\beta_1}{2} \frac{\partial^3}{\partial \tau^3}.$$

Furthermore, similarly as for b_r , b_i decays to zero for high frequencies, so that \mathcal{L}_i has no effect on the high-frequency components.

It is interesting to determine which operator, \mathcal{L}_r or \mathcal{L}_i , is the more important one. By scaling arguments, we get that $\omega^3 \beta_1$ is of the order of $(\omega l_c) \mu_0 l_c^2$, which is smaller than $\mu_0 \omega^2$ if $\omega l_c \ll 1$. As a result, the effective dispersion for small frequencies is usually smaller than the effective diffusion. Furthermore, we usually have $\beta_1 > 0$. This is the case, for instance, for a Gaussian autocorrelation function of the form $\gamma_0(x) = \exp(-\pi x^2/l_c^2)$. The length l_c is indeed the correlation length of the medium in the sense of (2.5). Besides, we have $\mu_0 = l_c/2$, and $\beta_1 = l_c^2/(2\pi)$. The fact that $\beta_1 > 0$ shows that the dispersion is reduced compared to the original one: the third-order dispersion coefficient, which is equal to $\beta_0/6$ in the absence of randomness, takes the value $\beta_0/6 - \beta_1/2$ in the presence of random topography. This dispersion reduction will be illustrated in the numerical simulations reported at the end of the paper. Note, however, that special configurations can be encountered that do not belong to the general case described above. One interesting case deserves a specific discussion. Let us consider for a while that the process n_0 is the derivative of a smooth stationary zero-mean random process ν such as a Gaussian random process with Gaussian autocorrelation function. We then have $\gamma_0(u) = -\partial_u^2 \mathbb{E}[\nu(0)\nu(u)]$, and $\mu_0 = 0$ while $\beta_1 = -\mathbb{E}[\nu(0)^2] < 0$. This shows that, in this very particular case, the dominant operator is the dispersion operator, and it enhances the original dispersion.

Our approach allows us to get the complete statistical distribution of the free surface wave, which gives more precise results than the mean-field approach. Indeed, by Proposition 3.2, the mean field $B_{\text{mf}}(\xi, \tau) = \lim_{\varepsilon \rightarrow 0} \mathbb{E}[B(\xi/\varepsilon^2, \tau + \xi/\varepsilon^2)]$ satisfies

$$(3.12) \quad \frac{\partial B_{\text{mf}}}{\partial \xi} = \mathcal{L}_{\text{mf}} B_{\text{mf}} + \frac{3\alpha_0}{4} B_{\text{mf}} \frac{\partial B_{\text{mf}}}{\partial \tau} + \frac{\beta_0}{6} \frac{\partial^3 B_{\text{mf}}}{\partial \tau^3},$$

where

$$(3.13) \quad \mathcal{L}_{\text{mf}} = \mathcal{L}_i + \mathcal{L}_r + \frac{b_0(0)}{4} \frac{\partial^2}{\partial \tau^2}.$$

The additional diffusion originates from the averaging with respect to the random time delay T_ξ defined by (3.7). In [23] the authors obtained (3.12)–(3.13) by applying

a multiscale expansion technique to the mean field. Our results clearly show that diffusion is overestimated by the mean-field approach and that only \mathcal{L}_r is a physical diffusion.

To sum up, in the general case where $\mu_0 > 0$, if the typical wavelength of the original pulse f is larger than the correlation radius of the medium, then the early steps of the effective evolution equation are those of the viscous KdV equation

$$(3.14) \quad \frac{\partial \tilde{B}_0}{\partial \xi} = \frac{\mu_0}{4} \frac{\partial^2 \tilde{B}_0}{\partial \tau^2} + \frac{3\alpha_0}{4} \tilde{B}_0 \frac{\partial \tilde{B}_0}{\partial \tau} + \left(\frac{\beta_0}{6} - \frac{\beta_1}{2} \right) \frac{\partial^3 \tilde{B}_0}{\partial \tau^3}.$$

In this case we have an eddy viscosity [34] which looks like a kinematic viscosity. Both forms of viscosity remove energy from the coherent wavefront in a diffusive-like manner. We can think of a low-pass Gaussian filter. However, the energy filtered by a kinematic viscosity is lost forever and cannot be recovered: it models an irreversible process. As discussed in a recent letter [15] the energy filtered by the eddy viscosity corresponds to a conversion of coherent energy transported by the front pulse into incoherent energy contained in the small wave fluctuations following the front pulse. The energy filtered by the eddy viscosity can be recovered along the coherent wavefront by a time-reversal recompression using a time-reversal mirror. This surprising result shows that the eddy viscosity models a reversible process. Therefore, although the kinematic and eddy viscosity appear with the same form, they are of a very different nature.

Finally, note that (3.14) may be valid only during the early steps of the wave propagation. Indeed, new wavelengths generated by the nonlinearity may lie in the tail of the function $b_0(2\omega)$, and it is then necessary to take into account the complete pseudodifferential operator, not only its expansion. Note also that we cannot consider the true white noise case, because a white noise does not fulfill the boundedness requirement that is necessary to ensure the convergence result. Indeed, the assumption $\mathbb{E}[n_0(0)^2] < \infty$ (and $\mathbb{E}[n'_0(0)^2] < \infty$) is important for the proof of the convergence result, and it is not fulfilled by the white noise whose variance is infinity. Nevertheless, qualitatively speaking, white noise disorder would affect the entire spectrum of the pulse as opposed to the case discussed here.

3.2. Rough topography. We now consider a specific case of rough topography to emphasize that the class of topographies that can be addressed by our theory is broader than those considered in the previous section. It is well known that stepped profiles, joining regions of different depths, is a difficult problem of interest, since this corresponds to waves propagating over, for instance, the continental shelf [9, 10]. Also many times stepped topographies are considered as an approximation strategy for arbitrary bottom slopes [10, 7]. Thus we will present a case of a randomly stepped profile for which certain statistical quantities can be computed explicitly. Moreover, as in the linear problems considered in [10, 7] we consider the wide-spacing hypothesis in the sense that the jumps are separated by a distance of order one.

Namely, in this section we assume that the topography is a rough, stepped profile, in the sense that the random process n_0 is bounded and satisfies $\mathbb{E}[n_0(0)^2] < \infty$, but it has jumps. For the sake of simplicity, we shall assume that n_0 can be modeled by

$$(3.15) \quad n_0(x) = n_\infty (-1)^{N_x},$$

where $(N_x)_{x \geq 0}$ is a Poisson process with intensity $1/l_c$. This means that (i) N_x takes integer values; (ii) the increments of the process are independent; and (iii) the

distribution of N_x is $\mathbb{P}(N_x = k) = \exp(-x/l_c)(x/l_c)^k k!$, $k \in \mathbb{N}$. As a result, the process n_0 is Markov, takes values in $\{-n_\infty, n_\infty\}$, and has mean zero and variance n_∞^2 , and its autocorrelation function is

$$\mathbb{E}[n_0(x_0)n_0(x_0 + x)] = n_\infty^2 \exp\left(-\frac{2|x|}{l_c}\right).$$

Note that l_c is indeed the correlation length of the medium in the sense of (2.5). Contrarily to the smooth topography case studied in the previous section, the metric process $M(\xi)$ here is different from $1 + \varepsilon n_0$ because the jumps of n_0 are smoothed. The analysis of the smoothing can be carried out by considering first the case where

$$n_{0,1}(x) = n_\infty \operatorname{sgn}(x),$$

which is an elementary jump from $-n_\infty$ to n_∞ . Using the Schwarz–Christoffel formula [30] we get the following representation for the corresponding metric coefficient:

$$M_1(\xi) = C \left(\frac{\cosh\left(\frac{\pi\xi}{2\sqrt{\beta_0}\varepsilon}\right)}{\cosh\left(\frac{\pi(\xi-a)}{2\sqrt{\beta_0}\varepsilon}\right)} \right)^{1/2},$$

where

$$C = \sqrt{1 - \varepsilon^2 n_\infty^2}, \quad a = \frac{2\sqrt{\beta_0}\varepsilon}{\pi} \ln\left(\frac{1 + \varepsilon n_\infty}{1 - \varepsilon n_\infty}\right).$$

An expansion with respect to ε gives to leading order

$$M_1(\xi) = 1 + \varepsilon n_\infty \tanh\left(\frac{\pi\xi}{2\sqrt{\beta_0}\varepsilon}\right),$$

which can also be written in the convolution form

$$(3.16) \quad M_1(\xi) = 1 + \varepsilon K^\varepsilon * n_{0,1}(\xi), \quad K^\varepsilon(\xi) = \frac{\pi}{4\sqrt{\beta_0}\varepsilon \cosh^2\left(\frac{\pi\xi}{2\sqrt{\beta_0}\varepsilon}\right)}.$$

Since the random process n_0 defined by (3.15) is stepwise constant and its jumps are separated by a distance of order one, the previous analysis gives the leading-order expression for the metric coefficient M :

$$(3.17) \quad M(\xi) = 1 + \varepsilon K^\varepsilon * n_0(\xi),$$

where K^ε is the kernel (3.16). The derivative of M has the form

$$M'(\xi) = \frac{\pi n_\infty}{2\sqrt{\beta_0}} \left\{ \frac{1}{2} \frac{1}{\cosh^2\left[\frac{\pi\xi}{2\sqrt{\beta_0}\varepsilon}\right]} + \sum_{j=1}^{\infty} \frac{(-1)^j}{\cosh^2\left[\frac{\pi(\xi-X_j)}{2\sqrt{\beta_0}\varepsilon}\right]} \right\},$$

where the X_j are the random positions of the jumps of n_0 . From a statistical point of view, $X_0 = 0$ and $(X_j - X_{j-1})_{j \geq 1}$ is a sequence of independent and identically distributed random variables with exponential distribution and mean l_c . The derivative $M'(\xi)$ is therefore a collection of alternating negative and positive peaks with the same sech^2 shape, amplitude of order 1, and width of order ε . Although the scaling

regime is different, the same analysis as in the previous section can be carried out, leading to the same result as stated in Proposition 3.2. The real and imaginary parts of the Fourier transform of the pseudodifferential operator \mathcal{L} here are given by

$$-\frac{b_r(2\omega)\omega^2}{4} = -\frac{n_\infty^2 l_c \omega^2}{8(1 + \omega^2 l_c^2)}, \quad -\frac{b_i(2\omega)\omega^2}{4} = -\frac{n_\infty^2 l_c^2 \omega^3}{8(1 + \omega^2 l_c^2)}.$$

Note that the diffusive and dispersive parts of the pseudodifferential operator do not vanish when $\omega l_c \gg 1$, but they behave like

$$-\frac{b_r(2\omega)\omega^2}{4} \rightarrow -\frac{n_\infty^2}{8l_c}, \quad -\frac{b_i(2\omega)\omega^2}{4} \rightarrow -\frac{n_\infty^2 \omega}{8}.$$

As a consequence, when the correlation length l_c of the random topography is larger than the pulse width, then the effective pulse front equation has the form of a KdV equation with damping:

$$(3.18) \quad \frac{\partial \tilde{B}_0}{\partial \xi} - \frac{n_\infty^2}{8} \frac{\partial \tilde{B}_0}{\partial \tau} = -\frac{n_\infty^2}{8l_c} \tilde{B}_0 + \frac{3\alpha_0}{4} \tilde{B}_0 \frac{\partial \tilde{B}_0}{\partial \tau} + \frac{\beta_0}{6} \frac{\partial^3 \tilde{B}_0}{\partial \tau^3}.$$

The analysis of the random topography of the form (3.15) shows that the regularization effect due to stochastic forcing is more important for a rough topography than for a smooth one. This analysis is also interesting because it allows an explicit characterization of the regularization effect of the pseudodamping. Indeed, in the special case $\beta_0 = 0$, a closed form expression for the solution of (3.18) can be obtained by the method of characteristics [36]

$$\frac{\partial \tilde{B}_0}{\partial \tau}(\xi, \tau) = \frac{\exp(-\frac{c\xi}{l_c})f'(\tau + c\xi)}{1 - \frac{3\alpha_0 l_c}{4c}[1 - \exp(-\frac{c\xi}{l_c})]f'(\tau + c\xi)},$$

where f is the initial pulse shape (supposed to be smooth) at $\xi = 0$, f' is its derivative, and $c = n_\infty^2/8$. This expression of the (derivative of the) solution is valid as long as the denominator does not vanish. As a consequence, the shock formation is determined by the value of the parameter

$$S := \frac{6\alpha_0 l_c}{n_\infty^2} \max_{\tau \in \mathbb{R}} f'(\tau).$$

(1) If $S > 1$, then a shock occurs at the propagation distance

$$\xi_s = \frac{8l_c}{n_\infty^2} \ln \left(\frac{S}{S - 1} \right).$$

(2) If $S \leq 1$, then the solution of (3.18) is global. The effective damping removes energy fast enough to prevent from the shock formation.

Note that the case $\beta_0 = 0$ is a limit case that is never reached in practice, so that shock formation can never be observed because of the presence of dispersion. However, it is a limit case that is mathematically well known and investigated, and it can be treated analytically. Besides, the parameter β_0 can be very small, and then it is interesting to study how damping competes with nonlinearity.

4. Large-amplitude, rapidly varying topography.

4.1. Statement of the main results. In this section we still write the small nonlinear and dispersion parameters as $\alpha = \varepsilon^2 \alpha_0$ and $\beta = \varepsilon^2 \beta_0$, but we assume that the random topography has a correlation length smaller than the wavelength. The suitable scaling that will give rise to a nontrivial asymptotic regime consists in taking

$$(4.1) \quad n(x) = \varepsilon^p n_0 \left(\frac{x}{\varepsilon^{2-2p}} \right),$$

where n_0 is a stationary random process with standard deviation and correlation length of order 1, and $p \in (3/8, 1/2)$. Equation (4.1) models a rapidly varying random topography.

1. The assumption $p < 1/2$ ensures that the correlation length ε^{2-2p} of the random bottom is much smaller than the scale ε of the smoothing kernel in (2.3). The smoothing effect then plays a primary role. Note that if $p > 1/2$, then the correlation length is much larger than the scale of the smoothing kernel, and the smoothing effect is negligible. The metric coefficient is of the form $M(\xi) = 1 + \varepsilon^p m(\xi/\varepsilon^{2-2p})$ with $m \simeq n_0$ to leading order. We then get the same results as in section 3.
2. The restriction $p > 3/8$ allows us to obtain a universal statistical description of the metric coefficient M , in the sense that it does not depend on the detail of the statistics of n_0 . When going to $p < 3/8$, the statistics become more complicated, as we shall see below.
3. The amplitude factor ε^p is chosen so that the integrated covariance of the random process n is of order ε^2 , i.e., of the same order as the dispersion and nonlinearity parameters. The effects of the random perturbations then become of order one after a propagation distance of order ε^{-2} .
4. In terms of smoothness we assume that there exists a constant $C \in (0, 1)$ such that $\|n_0\|_\infty \leq C$ almost surely, and we require n_0 to be differentiable with $\mathbb{E}[n_0'(0)^2] < \infty$. We also assume that the random process possesses strong mixing properties, more precisely, that it is ϕ -mixing with $\phi \in L^{1/2}$ (see [19, pp. 82–83]).

In this framework, the scale of variations of the metric coefficient $M(\xi)$ is different from the original scale of the topographic coefficient n , as shown by the following proposition. This new scale is imposed by the convolution of the fast topographic process with the scaled sech² function.

PROPOSITION 4.1. *The orography-dependent coefficient $M(\xi)$ in the case of a large-amplitude rapidly varying random topography (4.1) acquires Gaussian statistics in the limit $\varepsilon \rightarrow 0$, with the asymptotic autocorrelation function*

$$(4.2) \quad \frac{1}{\varepsilon} \mathbb{E} [(M(\xi_0) - 1)(M(\xi_0 + \varepsilon\xi) - 1)] \xrightarrow{\varepsilon \rightarrow 0} \gamma_m(\xi),$$

where

$$(4.3) \quad \gamma_m(x) = \frac{\pi\mu_0}{\sqrt{\beta_0}} \frac{\frac{\pi x}{2\sqrt{\beta_0}} \cosh(\frac{\pi x}{2\sqrt{\beta_0}}) - \sinh(\frac{\pi x}{2\sqrt{\beta_0}})}{\sinh^3(\frac{\pi x}{2\sqrt{\beta_0}})},$$

and μ_0 is the integrated correlation function of the random topography:

$$\mu_0 = \int_0^\infty \mathbb{E}[n_0(0)n_0(x)]dx.$$

Sections 4.2–4.3 are devoted to the proof of Proposition 4.1. Note that μ_0 is the only parameter that remains from the random topography. This result shows that the wave dynamics acquires a universal behavior driven by a random Gaussian process with the autocorrelation function (4.3). The power spectral density of this process, given by the Fourier transform of the autocorrelation function, is

$$\hat{\gamma}_0(k) = \mu_0 \left(\frac{\sqrt{\beta_0}k}{\sinh(\sqrt{\beta_0}k)} \right)^2 .$$

As a by-product of the analysis carried out in the proof of Proposition 4.1, we obtain the expansion of the averaged value of the metric coefficient $M(\xi)$ in the limit $\varepsilon \rightarrow 0$.

PROPOSITION 4.2. *The averaged value of the metric coefficient can be expanded as $\varepsilon \rightarrow 0$:*

$$(4.4) \quad \mathbb{E} [M(\xi)] = 1 - \varepsilon^{4p-1} \frac{\sqrt{\beta_0}}{2\pi} \int \hat{\gamma}_0(k) |k| dk + o(\varepsilon^{4p-1}),$$

where $\hat{\gamma}_0$ is given by (4.9).

This result can be used to prove a numerical observation reported in the literature and also to comment on the range of validity of Proposition 4.1. Note that the coefficient $\hat{\gamma}_0$ is the Fourier transform of the autocorrelation function of the process n_0 , which is nonnegative by the Wiener–Khinchine theorem. This shows that the first-order correction to the expectation of the metric coefficient is negative valued, which means that the effective bottom is located at a depth < 1 . The fact that a zero-mean varying random topography can give rise to a nonzero average depth through the conformal mapping was already pointed out in [28]. In our setting $p \in (3/8, 1/2)$, this effect is negligible. However, as $p \rightarrow 3/8$, the expansion (4.4) shows that the average value of $M - 1$ becomes of order $\varepsilon^{1/2}$, which is of the same order as the standard deviation of the asymptotic zero-mean Gaussian process described in Proposition 4.1. This remark shows that the situation becomes more complicated when $p \rightarrow 3/8$, and it will be addressed in a future work.

Finally, we go back to the wave propagation problem using the results above. If we focus our attention on the coherent front, then the picture becomes rather simple and qualitatively similar to the one encountered in the case of a small-amplitude slowly varying topography addressed in section 3. To summarize, up to a random time shift, the dynamics of the coherent front pulse is governed by a deterministic diffusive KdV-type equation whose diffusion coefficient depends only on the randomness through the parameter μ_0 .

PROPOSITION 4.3. *The front pulse $B^\varepsilon(\xi, \tau) := B(\xi/\varepsilon^2, \tau + \xi/\varepsilon^2)$ converges to $\tilde{B}(\xi, \tau) = \tilde{B}_0(\xi, \tau - T_\xi)$, where T_ξ is the random time shift defined by (3.7) and \tilde{B}_0 is the solution of the deterministic equation*

$$(4.5) \quad \frac{\partial \tilde{B}_0}{\partial \xi} = \frac{\mu_0}{4} \frac{\partial^2 \tilde{B}_0}{\partial \tau^2} + \frac{3\alpha_0}{4} \tilde{B}_0 \frac{\partial \tilde{B}_0}{\partial \tau} + \frac{\beta_0}{6} \frac{\partial^3 \tilde{B}_0}{\partial \tau^3} ,$$

starting from $\tilde{B}_0(0, \tau) = f(\tau)$.

The proof of Proposition 4.3 is given in subsection 4.4 in the linear case. Its nonlinear extension is then suggested by a heuristic argument. Note that the variance of the random time delay as well as the effective noise-induced diffusion depend only on the parameter μ_0 , which is the integrated autocorrelation function of the process n_0 .

4.2. Asymptotic analysis of the conformal mapping. The metric coefficient $M(\xi)$ is defined by (2.3). It is given by the convolution of a smooth explicit kernel with the composition of the random process n_0 and the real part of the conformal map $x(\xi, \zeta)$ evaluated at the unperturbed bottom $-\sqrt{\beta}$. The goal of this section is to get an asymptotic expansion of $x(\xi, -\sqrt{\beta})$ as $\varepsilon \rightarrow 0$. This requires us to analyze the conformal mapping introduced in [29, 30]. We start by considering the problem

$$(4.6) \quad \Delta \xi(x, y) = 0,$$

with the boundary condition $\xi_y = 0$ at $y = 0$ and

$$(4.7) \quad \xi_n = \xi_y + \sqrt{\beta} n'(x) \xi_x = 0 \text{ at } y = -\sqrt{\beta}(1 + n(x)).$$

To solve this problem in the asymptotic $\varepsilon \rightarrow 0$, we first replace the boundary condition at the random bottom $y = -\sqrt{\beta}(1 + n(x))$ by a boundary condition at the flat bottom $y = -\sqrt{\beta} = -\varepsilon\sqrt{\beta_0}$:

$$\xi_y + \sqrt{\beta_0} \varepsilon^{3p-1} n'_0 \left(\frac{x}{\varepsilon^{2-2p}} \right) \xi_x = R_1^\varepsilon + R_2^\varepsilon,$$

with

$$R_1^\varepsilon = \sqrt{\beta_0} \varepsilon^{1+p} n_0 \left(\frac{x}{\varepsilon^{2-2p}} \right) \int_0^1 \xi_{yy} \left(x, -\sqrt{\beta_0} \varepsilon \left(1 + \theta \varepsilon^p n_0 \left(\frac{x}{\varepsilon^{2-2p}} \right) \right) \right) d\theta,$$

$$R_2^\varepsilon = \beta_0 \varepsilon^{4p} n_0 n'_0 \left(\frac{x}{\varepsilon^{2-2p}} \right) \int_0^1 \xi_{xy} \left(x, -\sqrt{\beta_0} \varepsilon \left(1 + \theta \varepsilon^p n_0 \left(\frac{x}{\varepsilon^{2-2p}} \right) \right) \right) d\theta.$$

The corrective terms R_1^ε and R_2^ε are the Lagrange remainders of the Taylor expansions of ξ_y and $\sqrt{\beta_0} \varepsilon^{3p-1} n'_0 \left(\frac{x}{\varepsilon^{2-2p}} \right) \xi_x$ at $y = -\varepsilon\sqrt{\beta_0}$. The solution has the form

$$(4.8) \quad \xi(x, y) = \xi_0(x) + \xi_1(x, y) + \xi_r(x, y),$$

where $\xi_0(x) = x$ is the identity describing the conformal map in the absence of perturbation, and ξ_1 is the first-order corrective term satisfying the Laplace equation $\Delta \xi_1 = 0$, the boundary condition $\xi_{1y} = 0$ at $y = 0$, and the boundary condition $\xi_{1y} + \sqrt{\beta_0} \varepsilon^{3p-1} n'_0 \left(\frac{x}{\varepsilon^{2-2p}} \right) \xi_{0x} = 0$ at $y = -\sqrt{\beta_0} \varepsilon$. After a Fourier transform with respect to x , we find that

$$\xi_1(x, y) = \frac{i\sqrt{\beta_0} \varepsilon^{1+p}}{2\pi} \int \frac{\cosh(ky \varepsilon^{2p-2})}{\sinh(k\sqrt{\beta_0} \varepsilon^{2p-1})} e^{ik \frac{x}{\varepsilon^{2-2p}}} \hat{n}_0(k) dk,$$

where the Fourier transform is defined by

$$\hat{n}_0(k) = \int n_0(x) e^{-ikx} dx.$$

At the unperturbed bottom $y = -\sqrt{\beta_0} \varepsilon$ the random correction ξ_1 is a zero-mean process (in x) with autocorrelation function

$$\begin{aligned} \mathbb{E} \left[\xi_1(x_0, -\varepsilon\sqrt{\beta_0}) \xi_1(x_0 + \varepsilon^{2-2p} x, -\varepsilon\sqrt{\beta_0}) \right] &= \frac{\beta_0 \varepsilon^{2+2p}}{2\pi} \int \hat{\gamma}_0(k) e^{ikx} dk + o(\varepsilon^{2+2p}) \\ &= \beta_0 \varepsilon^{2+2p} \gamma_0(x) + o(\varepsilon^{2+2p}), \end{aligned}$$

where

$$(4.9) \quad \gamma_0(x) = \mathbb{E}[n_0(x_0)n_0(x_0 + x)]$$

is the autocorrelation function of the process n_0 , and $\hat{\gamma}_0$ is its Fourier transform, which is proportional to the power spectral density of the random process n_0 :

$$\mathbb{E} [\hat{n}_0(k)\overline{\hat{n}_0(k + k')}] = 2\pi\hat{\gamma}_0(k)\delta(k').$$

This result also shows that $R_1^\varepsilon = O(\varepsilon^{6p-2})$ and $R_2^\varepsilon = O(\varepsilon^{9p-3})$, which means that the terms R_j^ε are higher-order corrections in (4.7) in the case $p > 1/3$. It also shows that $\xi_r = O(\varepsilon^{4p})$. Inverting relation (4.8) at the undisturbed bottom, we have

$$(4.10) \quad x(\xi, -\varepsilon\sqrt{\beta_0}) = \xi + \varepsilon^{1+p}X^\varepsilon(\xi) + O(\varepsilon^{4p}),$$

with $X^\varepsilon(\xi)$ a fast varying (at scale ε^{2-2p}) zero-mean process with standard deviation of order one given by

$$(4.11) \quad X^\varepsilon(\xi) = -\frac{i\sqrt{\beta_0}}{2\pi} \int \frac{\cosh(k\sqrt{\beta_0}\varepsilon^{2p-1})}{\sinh(k\sqrt{\beta_0}\varepsilon^{2p-1})} e^{ik\frac{\xi}{\varepsilon^{2-2p}}} \hat{n}_0(k)dk.$$

This expression will be used in the next section to study the asymptotic properties of the metric coefficient.

4.3. Asymptotic analysis of the metric coefficient. In this section we prove Propositions 4.1 and 4.2. First note that, from (2.3) and (4.10), the expected value of the metric coefficient M can be expanded as

$$\mathbb{E} [M(\xi)] = 1 + \frac{\pi\varepsilon^{4p-2}}{4\sqrt{\beta_0}} \int \frac{\mathbb{E}[n'_0(\xi_0\varepsilon^{2p-2})X^\varepsilon(\xi_0)]}{\cosh^2\left[\frac{\pi}{2\sqrt{\beta_0}\varepsilon}(\xi - \xi_0)\right]} d\xi_0 + \dots,$$

where X^ε is defined by (4.11). In the asymptotic $\varepsilon \rightarrow 0$, we obtain (4.4), which proves Proposition 4.2.

In order to prove Proposition 4.1, we are going to show that, for any ξ' and for any smooth test function g , the sequence of random variables

$$(4.12) \quad G_{\xi'}^\varepsilon(g) = \int \left[\frac{1}{\sqrt{\varepsilon}} (M(\xi' + \varepsilon\xi) - 1) \right] g(\xi)d\xi$$

converges in distribution as $\varepsilon \rightarrow 0$ to a Gaussian random variable whose variance can be identified. This convergence result will be obtained by computing the limiting moments of $G_{\xi'}^\varepsilon(g)$.

From the definition (2.3) of the coefficient M , the complete expression of $G_{\xi'}^\varepsilon(g)$ is

$$(4.13) \quad G_{\xi'}^\varepsilon(g) = \frac{\pi}{4\sqrt{\beta_0}\varepsilon^{3/2-p}} \int \int \frac{n_0\left(\frac{x(\xi_0)}{\varepsilon^{2-2p}}\right)g(\xi)}{\cosh^2\left[\frac{\pi}{2\sqrt{\beta_0}\varepsilon}(\xi_0 - \xi' - \varepsilon\xi)\right]} d\xi_0 d\xi.$$

By (4.10), we first note that

$$\frac{x(\xi_0)}{\varepsilon^{2-2p}} = \frac{\xi_0}{\varepsilon^{2-2p}} + O(\varepsilon^{3p-1}).$$

Since n'_0 can be bounded (in quadratic mean), it is possible to substitute $n_0(\frac{\xi_0}{\varepsilon^{2-2p}})$ for $n_0(\frac{x(\xi_0)}{\varepsilon^{2-2p}})$ in (4.13) up to an error of order $\varepsilon^{p-3/2} \times \varepsilon^{3p-1} \times \varepsilon = \varepsilon^{4p-3/2}$. Since $p > 3/8$, this error is negligible, and we get that, to leading order in ε ,

$$G_{\xi'}^\varepsilon(g) = \frac{\pi}{4\sqrt{\beta_0}\varepsilon^{3/2-p}} \int \int \frac{n_0(\frac{\xi_0}{\varepsilon^{2-2p}})g(\xi)}{\cosh^2 \left[\frac{\pi}{2\sqrt{\beta_0}\varepsilon}(\xi_0 - \xi' - \varepsilon\xi) \right]} d\xi_0 d\xi.$$

We next perform the change of variable $\xi_0 \mapsto u_0 = (\xi_0 - \xi')/\varepsilon^{2-2p}$:

$$G_{\xi'}^\varepsilon(g) = \frac{\pi\varepsilon^{1/2-p}}{4\sqrt{\beta_0}} \int \int \frac{n_0(\frac{\xi'}{\varepsilon^{2-2p}} + u_0)g(\xi)}{\cosh^2 \left[\frac{\pi}{2\sqrt{\beta_0}}(\varepsilon^{1-2p}u_0 - \xi) \right]} du_0 d\xi.$$

We denote $\varepsilon' = \varepsilon^{1-2p}$. Remember that $p < 1/2$ so that ε' goes to zero as ε goes to zero. We fix $q \in \mathbb{N}$ and consider the $2q$ th moment. Using the stationarity of the process n_0 , we have

$$\mathbb{E} [G_{\xi'}^\varepsilon(g)^{2q}] = \left(\frac{\pi^2 \varepsilon'}{16\beta_0} \right)^q \int_{\xi_1, \dots, \xi_{2q}} \int_{u_1, \dots, u_{2q}} \frac{\mathbb{E}[\prod_{j=1}^{2q} n_0(u_j)] \prod_j g(\xi_j)}{\prod_j \cosh^2 \left[\frac{\pi}{2\sqrt{\beta_0}}(\varepsilon' u_j - \xi_j) \right]} du_j d\xi_j.$$

The integrand in this equation is symmetric with respect to the set $(u_i)_{i=1, \dots, 2q}$, and so we can write

$$\mathbb{E} [G_{\xi'}^\varepsilon(g)^{2q}] = \left(\frac{\pi^2 \varepsilon'}{16\beta_0} \right)^q (2q)! \int_{\xi_1, \dots, \xi_{2q}} \int_{u_1 < \dots < u_{2q}} \frac{\mathbb{E}[\prod_{j=1}^{2q} n_0(u_j)] \prod_j g(\xi_j)}{\prod_j \cosh^2 \left[\frac{\pi}{2\sqrt{\beta_0}}(\varepsilon' u_j - \xi_j) \right]} du_j d\xi_j.$$

By setting $u_{2i-1} = v_{2i-1}/\varepsilon'$ and $u_{2i} = u_{2i-1} + v_{2i}$,

$$\begin{aligned} \mathbb{E} [G_{\xi'}^\varepsilon(g)^{2q}] &= \left(\frac{\pi^2}{16\beta_0} \right)^q (2q)! \int_{\xi_1, \dots, \xi_{2q}} \int_{v_1 < v_1 + \varepsilon' v_2 < v_3 < v_3 + \varepsilon' v_4 < \dots < v_{2p-1} < v_{2q-1} + \varepsilon' v_{2q}} \\ &\times \frac{\mathbb{E} \left[\prod_{i=1}^q n_0\left(\frac{v_{2i-1}}{\varepsilon'}\right) n_0\left(\frac{v_{2i-1}}{\varepsilon'} + v_{2i}\right) \prod_{i=1}^q g(\xi_{2i-1}) g(\xi_{2i}) \right]}{\prod_{i=1}^q \cosh^2 \left[\frac{\pi}{2\sqrt{\beta_0}}(v_{2i-1} - \xi_{2i-1}) \right] \cosh^2 \left[\frac{\pi}{2\sqrt{\beta_0}}(v_{2i-1} + \varepsilon' v_{2i} - \xi_{2i}) \right]} \prod_{i=1}^{2q} dv_i d\xi_i. \end{aligned}$$

We now use the strong mixing properties of the process n_0 , which implies that, for any $v_1 < v_3 < \dots < v_{2q-1}$ and for any $v_2, \dots, v_{2q} \geq 0$,

$$\mathbb{E} \left[\prod_{i=1}^q n_0 \left(\frac{v_{2i-1}}{\varepsilon'} \right) n_0 \left(\frac{v_{2i-1}}{\varepsilon'} + v_{2i} \right) \right] \xrightarrow{\varepsilon \rightarrow 0} \prod_{i=1}^q \gamma_0(v_{2i}),$$

where $\gamma_0(x) = \mathbb{E}[n_0(x_0 + x)n_0(x_0)]$. As a result,

$$\begin{aligned} \mathbb{E} [G_{\xi'}^\varepsilon(g)^{2q}] &\xrightarrow{\varepsilon \rightarrow 0} \left(\frac{\pi^2}{16\beta_0} \right)^q (2q)! \int_{\xi_1, \dots, \xi_{2q}} \int_{v_1 < v_3 < \dots < v_{2q-1}} \int_{v_2 > 0, \dots, v_{2q} > 0} \\ &\times \prod_{i=1}^q \frac{\gamma_0(v_{2i})g(\xi_{2i-1})g(\xi_{2i})}{\cosh^2 \left[\frac{\pi}{2\sqrt{\beta_0}}(v_{2i-1} - \xi_{2i-1}) \right] \cosh^2 \left[\frac{\pi}{2\sqrt{\beta_0}}(v_{2i-1} - \xi_{2i}) \right]} dv_{2i-1} dv_{2i} d\xi_{2i-1} d\xi_{2i}. \end{aligned}$$

The multiple integral is symmetric with respect to the set $(v_{2i-1})_{i=1,\dots,q}$, and so we can write

$$\mathbb{E} [G_{\xi'}^\varepsilon(g)^{2q}] \xrightarrow{\varepsilon \rightarrow 0} \left(\frac{\pi^2}{16\beta_0}\right)^q \frac{(2q)!}{q!} \int_{\xi_1, \dots, \xi_{2q}} \int_{v_1, v_3, \dots, v_{2q-1}} \int_{v_2 > 0, \dots, v_{2q} > 0} \\ \times \prod_{i=1}^q \frac{\gamma_0(v_{2i})g(\xi_{2i-1})g(\xi_{2i})}{\cosh^2\left[\frac{\pi}{2\sqrt{\beta_0}}(v_{2i-1} - \xi_{2i-1})\right] \cosh^2\left[\frac{\pi}{2\sqrt{\beta_0}}(v_{2i-1} - \xi_{2i})\right]} dv_{2i-1} dv_{2i} d\xi_{2i-1} d\xi_{2i}.$$

This multiple integral can now be factorized:

$$\mathbb{E} [G_{\xi'}^\varepsilon(g)^{2q}] \xrightarrow{\varepsilon \rightarrow 0} \left(\frac{\pi^2}{16\beta_0}\right)^q \frac{(2q)!}{q!} \\ \times \left(\int_{v_1} \int_{v_2 > 0} \int_{\xi_1, \xi_2} \frac{\gamma_0(v_2)g(\xi_1)g(\xi_2)}{\cosh^2\left[\frac{\pi}{2\sqrt{\beta_0}}(v_1 - \xi_1)\right] \cosh^2\left[\frac{\pi}{2\sqrt{\beta_0}}(v_1 - \xi_2)\right]} dv_1 dv_2 d\xi_1 d\xi_2 \right)^q.$$

By integrating the integral with respect to v_1 and v_2 , we get

$$(4.14) \quad \mathbb{E} [G_{\xi'}^\varepsilon(g)^{2q}] \xrightarrow{\varepsilon \rightarrow 0} \frac{(2q)!}{2^q q!} \times \left(\int_{\xi_1, \xi_2} \gamma_m(\xi_1 - \xi_2)g(\xi_1)g(\xi_2) d\xi_1 d\xi_2 \right)^q,$$

where γ_m is given by (4.3).

Let us now consider an odd moment of the form $\mathbb{E}[G_{\xi'}^\varepsilon(g)^{2q+1}]$, where q is a nonnegative integer. This moment involves the expectation of the product of an odd number of terms $n_0(x(\xi')/\varepsilon' + u_i)$, and following the same lines as the previous analysis, we get that this expectation converges to 0 as $\varepsilon \rightarrow 0$, so that we obtain

$$(4.15) \quad \mathbb{E} [G_{\xi'}^\varepsilon(g)^{2q+1}] \xrightarrow{\varepsilon \rightarrow 0} 0.$$

The limits (4.14)–(4.15) are the moments of a zero-mean Gaussian random variable with variance $\int_{\xi_1, \xi_2} \gamma_m(\xi_1 - \xi_2)g(\xi_1)g(\xi_2) d\xi_1 d\xi_2$; thus $G_{\xi'}^\varepsilon(g)$ converges in distribution to this random variable. This holds true for any test function g . As a result, this shows that $(\varepsilon^{-1/2}(M(\xi' + \varepsilon\xi) - 1))_{-\infty < \xi < \infty}$ converges to a Gaussian process. The limiting Gaussian process has zero mean and its autocorrelation function is γ_m .

4.4. Asymptotic analysis of the front pulse. As shown in the previous section, in the regime where the random topographic coefficient $n(x)$ has the form (4.1) with $p \in (3/8, 1/2)$, the metric coefficient M is asymptotically Gaussian distributed with the autocorrelation function (4.2)–(4.3). Accordingly we can write

$$(4.16) \quad M(\xi) = 1 + \varepsilon^{1/2} m \left(\frac{\xi}{\varepsilon} \right),$$

where m is a zero-mean smooth stationary random process with the autocorrelation function γ_m . The variance of m is $\mathbb{E}[m(0)^2] = \gamma_m(0) = \pi\mu_0/(3\sqrt{\beta_0})$. We also know that m is Gaussian distributed, but this hypothesis is not used in the derivation of the results of this section. The expression (4.16) is the leading-order term of the random coefficient $M(\xi)$. As is usual in the asymptotic analysis of randomly forced ODEs, the higher-order zero-mean corrections play no role and vanish in the limit $\varepsilon \rightarrow 0$. The deterministic corrections like (4.4) survive in the limit $\varepsilon \rightarrow 0$, and here they take

the form of a deterministic shift. This can be explained by the fact that the average bottom, and therefore the average velocity, are modified. We will not discuss this point further, as we are mainly interested in the wave deformation in this paper.

We now revisit the derivation of the effective equation for the front pulse in the case where the metric coefficient has the form (4.16). We first expand the system by keeping the leading-order terms in ε (i.e., those which play a role for propagation distances of the order of ε^{-2}):

$$\begin{aligned}
 \frac{\partial}{\partial \xi} \begin{pmatrix} A \\ B \end{pmatrix} &= Q(\xi) \frac{\partial}{\partial t} \begin{pmatrix} A \\ B \end{pmatrix} + \frac{1}{2\varepsilon^{1/2}} m' \left(\frac{\xi}{\varepsilon} \right) \begin{pmatrix} 1 & -1 \\ -1 & 1 \end{pmatrix} \begin{pmatrix} A \\ B \end{pmatrix} \\
 &+ \varepsilon^2 \frac{\alpha_0}{4} \begin{pmatrix} 3A+B & 0 \\ 0 & A+3B \end{pmatrix} \frac{\partial}{\partial t} \begin{pmatrix} A \\ B \end{pmatrix} \\
 (4.17) \quad &+ \varepsilon^2 \frac{\beta_0}{6} \begin{pmatrix} -1 & 0 \\ 0 & 1 \end{pmatrix} \frac{\partial^3}{\partial t^3} \begin{pmatrix} A \\ B \end{pmatrix} + \varepsilon^{1/2} \frac{\beta_0}{12} m'' \left(\frac{\xi}{\varepsilon} \right) \begin{pmatrix} -1 & 1 \\ -1 & 1 \end{pmatrix} \frac{\partial}{\partial t} \begin{pmatrix} A \\ B \end{pmatrix},
 \end{aligned}$$

where

$$(4.18) \quad Q(\xi) = \begin{pmatrix} 1 + \frac{\varepsilon^{1/2}}{2} m \left(\frac{\xi}{\varepsilon} \right) & \frac{\varepsilon^{1/2}}{2} m \left(\frac{\xi}{\varepsilon} \right) \\ -\frac{\varepsilon^{1/2}}{2} m \left(\frac{\xi}{\varepsilon} \right) & -1 - \frac{\varepsilon^{1/2}}{2} m \left(\frac{\xi}{\varepsilon} \right) \end{pmatrix}.$$

The third and fourth terms (nonlinear and dispersive) of the right-hand side of (4.17) are similar to the ones appearing in (3.4), but the other terms are rather different. In particular the second term involves highly fluctuating random components, with amplitudes of order $\varepsilon^{-1/2}$, and the asymptotic analysis requires more elaborate tools than in the slowly varying case addressed in the previous section, where the amplitude of the random fluctuations was of order ε . An efficient and rigorous study can be performed in absence of nonlinearity, and we present this study below.

We assume for a while that $\alpha_0 = 0$. We apply a Fourier transform with respect to time,

$$(4.19) \quad \hat{A}(\xi, \omega) = \int A(\xi, t) e^{i\omega t} dt, \quad \hat{B}(\xi, \omega) = \int B(\xi, t) e^{i\omega t} dt,$$

so that the PDE (4.17) can be reduced to an infinite set of ODEs for the modes \hat{A} and \hat{B} :

$$\begin{aligned}
 \frac{\partial}{\partial \xi} \begin{pmatrix} \hat{A} \\ \hat{B} \end{pmatrix} &= \left\{ i\omega Q(\xi) + \frac{1}{2\sqrt{\varepsilon}} m' \left(\frac{\xi}{\varepsilon} \right) \begin{pmatrix} 1 & -1 \\ -1 & 1 \end{pmatrix} \right. \\
 (4.20) \quad &\left. - i\omega^3 \varepsilon^2 \frac{\beta_0}{6} \begin{pmatrix} -1 & 0 \\ 0 & 1 \end{pmatrix} + i\omega \varepsilon^{1/2} \frac{\beta_0}{12} m'' \left(\frac{\xi}{\varepsilon} \right) \begin{pmatrix} -1 & 1 \\ -1 & 1 \end{pmatrix} \right\} \begin{pmatrix} \hat{A} \\ \hat{B} \end{pmatrix}.
 \end{aligned}$$

The boundary conditions corresponding to a right-going pulse coming from the homogeneous half-space $\xi < 0$ are

$$\hat{B}(0, \omega) = \hat{f}(\omega), \quad \hat{A}(L/\varepsilon^2, \omega) = 0.$$

The problem, from the analytic point of view, is very simple because each frequency-dependent pair of ODEs is uncoupled (from the rest) and linear. However, from the statistical point of view, these ODEs are coupled because they share the same process m (and its derivatives). The analysis of the correlation between different frequency components plays a central role in the convergence result.

We next rescale the propagation distances and introduce the left- and right-going modes centered along the deterministic characteristic lines:

$$\hat{A}_1^\varepsilon(\xi, \omega) = \hat{A}\left(\frac{\xi}{\varepsilon^2}, \omega\right) \exp\left(-i\omega \frac{\xi}{\varepsilon^2}\right), \quad \hat{B}_1^\varepsilon(\xi, \omega) = \hat{B}\left(\frac{\xi}{\varepsilon^2}, \omega\right) \exp\left(i\omega \frac{\xi}{\varepsilon^2}\right),$$

so that the system now has the form

$$\begin{aligned} \frac{\partial}{\partial \xi} \begin{pmatrix} \hat{A}_1^\varepsilon \\ \hat{B}_1^\varepsilon \end{pmatrix} &= \left\{ \frac{1}{2\varepsilon^{5/2}} m' \left(\frac{\xi}{\varepsilon^3} \right) \begin{pmatrix} 1 & -e^{-2i\omega \frac{\xi}{\varepsilon^2}} \\ -e^{2i\omega \frac{\xi}{\varepsilon^2}} & 1 \end{pmatrix} \right. \\ &\quad + \frac{i\omega}{2\varepsilon^{3/2}} m \left(\frac{\xi}{\varepsilon^3} \right) \begin{pmatrix} 1 & e^{-2i\omega \frac{\xi}{\varepsilon^2}} \\ -e^{2i\omega \frac{\xi}{\varepsilon^2}} & -1 \end{pmatrix} - \frac{i\omega^3 \beta_0}{6} \begin{pmatrix} -1 & 0 \\ 0 & 1 \end{pmatrix} \\ &\quad \left. + \frac{i\omega \beta_0}{12\varepsilon^{3/2}} m'' \left(\frac{\xi}{\varepsilon^3/2} \right) \begin{pmatrix} -1 & e^{-2i\omega \frac{\xi}{\varepsilon^2}} \\ -e^{2i\omega \frac{\xi}{\varepsilon^2}} & 1 \end{pmatrix} \right\} \begin{pmatrix} \hat{A}_1^\varepsilon \\ \hat{B}_1^\varepsilon \end{pmatrix}. \end{aligned} \tag{4.21}$$

The first term of the right-hand side, of the form $\varepsilon^{-5/2} q(\xi/\varepsilon^3)$, is not written in a form suitable for the application of a diffusion-approximation theorem, which requires a scaled random term of the form $\varepsilon^{-p/2} q(\xi/\varepsilon^p)$. It is possible to rewrite the first term in a more convenient form. Noting that

$$\begin{aligned} \frac{1}{\varepsilon^{5/2}} m' \left(\frac{\xi}{\varepsilon^3} \right) e^{-2i\omega \frac{\xi}{\varepsilon^2}} &= \frac{d}{d\xi} \left\{ \varepsilon^{1/2} m \left(\frac{\xi}{\varepsilon^3} \right) e^{-2i\omega \frac{\xi}{\varepsilon^2}} \right\} + \frac{2i\omega}{\varepsilon^{3/2}} m \left(\frac{\xi}{\varepsilon^3} \right) e^{-2i\omega \frac{\xi}{\varepsilon^2}}, \\ \frac{1}{\varepsilon^{5/2}} m' \left(\frac{\xi}{\varepsilon^3} \right) e^{2i\omega \frac{\xi}{\varepsilon^2}} &= \frac{d}{d\xi} \left\{ \varepsilon^{1/2} m \left(\frac{\xi}{\varepsilon^3} \right) e^{2i\omega \frac{\xi}{\varepsilon^2}} \right\} - \frac{2i\omega}{\varepsilon^{3/2}} m \left(\frac{\xi}{\varepsilon^3} \right) e^{2i\omega \frac{\xi}{\varepsilon^2}}, \end{aligned}$$

we can rewrite the system as

$$\frac{\partial}{\partial \xi} \begin{pmatrix} \hat{A}_1^\varepsilon \\ \hat{B}_1^\varepsilon \end{pmatrix} = [M^\varepsilon(\xi) + N^\varepsilon(\xi)] \begin{pmatrix} \hat{A}_1^\varepsilon \\ \hat{B}_1^\varepsilon \end{pmatrix} - \frac{i\omega^3 \beta_0}{6} \begin{pmatrix} -1 & 0 \\ 0 & 1 \end{pmatrix} \begin{pmatrix} \hat{A}_1^\varepsilon \\ \hat{B}_1^\varepsilon \end{pmatrix}, \tag{4.22}$$

where

$$\begin{aligned} M^\varepsilon(\xi) &= \begin{pmatrix} M_1^\varepsilon(\xi) & M_2^\varepsilon(\xi) \\ M_2^\varepsilon(\xi) & M_1^\varepsilon(\xi) \end{pmatrix}, & N^\varepsilon(\xi) &= \begin{pmatrix} N_1^\varepsilon(\xi) & N_2^\varepsilon(\xi) \\ N_2^\varepsilon(\xi) & N_1^\varepsilon(\xi) \end{pmatrix}, \\ M_1^\varepsilon(\xi) &= \frac{i\omega}{2\varepsilon^{3/2}} \left[m \left(\frac{\xi}{\varepsilon^3} \right) - \frac{\beta_0}{6} m'' \left(\frac{\xi}{\varepsilon^3} \right) \right], & N_1^\varepsilon(\xi) &= \frac{\varepsilon^{1/2}}{2} \frac{d}{d\xi} \left\{ m \left(\frac{\xi}{\varepsilon^3} \right) \right\}, \\ M_2^\varepsilon(\xi) &= \frac{-i\omega}{2\varepsilon^{3/2}} \left[m \left(\frac{\xi}{\varepsilon^3} \right) - \frac{\beta_0}{6} m'' \left(\frac{\xi}{\varepsilon^3} \right) \right] e^{-2i\omega \frac{\xi}{\varepsilon^2}}, & N_2^\varepsilon(\xi) &= -\frac{\varepsilon^{1/2}}{2} \frac{d}{d\xi} \left\{ m \left(\frac{\xi}{\varepsilon^3} \right) e^{-2i\omega \frac{\xi}{\varepsilon^2}} \right\}. \end{aligned}$$

Note that the scaling of the matrix M^ε is appropriate for the application of an diffusion-approximation theorem, while the matrix N^ε is the derivative of a process of order $\sqrt{\varepsilon}$.

The quantity that we are interested in is the front pulse:

$$B \left(\frac{L}{\varepsilon^2}, \frac{L}{\varepsilon^2} + t \right) = \frac{1}{2\pi} \int \hat{B}_1 \left(\frac{L}{\varepsilon^2}, \omega \right) e^{-i\omega t} d\omega. \tag{4.23}$$

We thus recover the situation studied in [6], which dealt with the hyperbolic acoustic equations. However, there are three differences:

(1) The nondiagonal terms in the matrix $M^\varepsilon(\xi)$ have components $\beta_0 m''$. This difference does not present any difficulty, and the analysis goes exactly along the same lines as in absence of these terms.

(2) There exists a second matrix N^ε (which was absent in [6]). This matrix can be incorporated into the convergence result, and it turns out that it gives a vanishing contribution in the asymptotic $\varepsilon \rightarrow 0$ because it is the derivative of a process with amplitude $\sqrt{\varepsilon}$.

(3) The scalings are different from the ones encountered in [6]. In the paper [6], the scaled ODE is of the form

$$\frac{dX^\varepsilon}{dz} = \frac{1}{\varepsilon} F\left(q\left(\frac{z}{\varepsilon^2}\right), \frac{z}{\varepsilon}, X^\varepsilon\right),$$

where q is a stationary random process, and $(q, h, x) \mapsto F(q, h, x)$ is a smooth function, periodic with respect to h , and satisfying the centering condition $\mathbb{E}[F(q(0), h, x)] = 0$ for all h and x . The asymptotic of the solution X^ε of this equation is given by a standard diffusion-approximation theorem [32, 33]. In our case, we can set $\tilde{\varepsilon} = \varepsilon^{3/2}$ so that the ODE is of the form

$$\frac{dX^{\tilde{\varepsilon}}}{dz} = \frac{1}{\tilde{\varepsilon}} F\left(q\left(\frac{z}{\tilde{\varepsilon}^2}\right), \frac{z}{\tilde{\varepsilon}^{2/3}}, X^{\tilde{\varepsilon}}\right),$$

with $X^{\tilde{\varepsilon}} = (\hat{A}_1^{\tilde{\varepsilon}}, \hat{B}_1^{\tilde{\varepsilon}})$, $q = (m, m'')$, and F is given by (4.22). We can then make use of the generalized multiscale approximation-diffusion theorem given in [14] to get the limit. Finally, we obtain that $B(L/\varepsilon^2, \tau + L/\varepsilon^2)$ converges as $\varepsilon \rightarrow 0$ to the process

$$\frac{1}{2\pi} \int \hat{f}(\omega) e^{i\omega \frac{\sqrt{\mu_m}}{\sqrt{2}} W_L - \omega^2 \frac{\mu_m}{4} L - i\omega^3 \frac{\beta_0}{6} L} e^{-i\omega\tau} d\omega,$$

where W_L is a standard Brownian motion, and

$$\mu_m = \int_0^\infty \mathbb{E} \left[\left(m(0) - \frac{\beta_0}{6} m''(0) \right) \left(m(u) - \frac{\beta_0}{6} m''(u) \right) \right] du.$$

Using the relations $\mathbb{E}[m''(0)m(u)] = \mathbb{E}[m(0)m''(u)] = \gamma_m''(u)$ and $\mathbb{E}[m''(0)m''(u)] = \gamma_m''''(u)$, we get that

$$(4.24) \quad \mu_m = \int_0^\infty \gamma_m(u) du + \frac{\beta_0}{3} \gamma_m'(0) - \frac{\beta_0^2}{36} \gamma_m''(0) = \int_0^\infty \gamma_m(u) du.$$

Here we have also used the fact that the autocorrelation function γ_m is a smooth even function, so that the odd-order derivatives of γ_m at 0 are vanishing. Using the explicit expression (4.3) of γ_m and integrating (4.24), we find that μ_m is equal to μ_0 , which is the integrated autocorrelation function of the process n_0 describing the fluctuations of the bottom of the channel. Going back to the time domain and taking into account the nonlinear term, we get Proposition 4.3. Therefore, the proof is complete in the linear case $\alpha = 0$ but not in the general case $\alpha > 0$. Indeed, the nonlinearity is not easy to manipulate in the Fourier domain. However, in the scaled regime addressed in this section, the nonlinearity is of order one, and so we can expect and conjecture that the result is true and observe it numerically, as shown in section 6.

5. Solitary pulse dynamics. In this section we study the front pulse dynamics driven by the effective equation (3.14) or (4.5):

$$(5.1) \quad \frac{\partial B}{\partial \xi} = \frac{\mu}{4} \frac{\partial^2 B}{\partial \tau^2} + \frac{3\alpha}{4} B \frac{\partial B}{\partial \tau} + \frac{\beta}{6} \frac{\partial^3 B}{\partial \tau^3},$$

and we focus our attention on the role of nonlinearity. Indeed, the unperturbed KdV equation ((5.1) with $\mu = 0$) supports soliton solutions, and it has been recognized in different situations that the soliton dynamics in the presence of random perturbations can be quite different from the dynamics of a small-amplitude pulse with the same profile (see, for instance, the review [2] and the references therein). For the sake of a quantitative analysis we introduce the pulse energy, or L^2 -norm, $E(\xi) = \int B^2(\xi, \tau) d\tau$.

5.1. Linear regime. We first study the pulse dynamics in the absence of nonlinearity and dispersion, that is, the heat equation (5.1) with $\alpha = \beta = 0$. We consider a sech^2 profile

$$f(\tau) = a_0 \text{sech}^2(\kappa_0 \tau)$$

with amplitude a_0 and energy $E_0 = 4a_0^2/(3\kappa_0)$. We can solve the effective equation in the Fourier domain, and using the Fourier representations of the pulse amplitude and energy

$$a(\xi) = \frac{1}{2\pi} \int \hat{B}(\xi, \omega) d\omega, \quad E(\xi) = \frac{1}{2\pi} \int |\hat{B}|^2(\xi, \omega) d\omega,$$

we get that the pulse amplitude and energy evolve as

$$(5.2) \quad a(\xi) = a_0 F\left(\frac{\xi}{\xi_0}\right), \quad E(\xi) = E_0 G\left(\frac{\xi}{\xi_0}\right), \quad \xi_0 = \frac{1}{\mu \kappa_0^2},$$

where

$$(5.3) \quad F(Z) = \frac{1}{2} \int e^{-\frac{zw^2}{4}} \frac{w}{\sinh(\frac{\pi w}{2})} dw, \quad G(Z) = \frac{3\pi}{8} \int e^{-\frac{zw^2}{2}} \frac{w^2}{\sinh^2(\frac{\pi w}{2})} dw.$$

We have $F(0) = 1$ and $F'(0) = -1/2$, which give an estimate of the initial decay rate of the sech^2 pulse amplitude.

It is also possible to study the linear pulse dynamics in the presence of dispersion, that is, the heat equation (5.1) with $\alpha = 0$ and $\beta > 0$. The idea is just to take the Fourier transform of (5.1) and to write the solution in the Fourier domain

$$\hat{B}(\xi, \omega) = \hat{f}(\omega) \exp\left(-\frac{\mu\omega^2\xi}{4} - i\frac{\beta\omega^3\xi}{6}\right).$$

The ω^3 term is related to the dispersive Airy kernel described in [11, 25]. However, it is not fair to compare the linear pulse dynamics in the presence of dispersion with the soliton dynamics in the presence of dispersion and nonlinearity, because the linear pulse will decay dramatically because of dispersion, even in the absence of random topography.

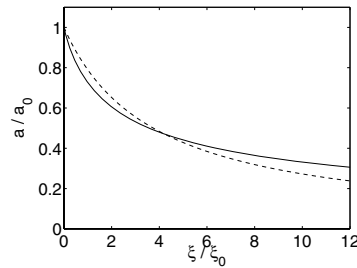


FIG. 5.1. Pulse amplitude versus propagation distance for a soliton in the presence of nonlinearity, dispersion, and randomness (dashed lines) and for a sech^2 pulse in the presence of randomness and in the absence of nonlinearity and dispersion (solid line). Here $\xi_0 = 1/(\mu\kappa_0^2)$. The crossing of the two lines occurs at the critical distance $4.25\xi_0$, when the pulse amplitude has been reduced by about 50%.

5.2. Soliton decay. We now assume that the initial pulse corresponds to a soliton solution of the unperturbed KdV equation ((5.1) with $\mu = 0$):

$$f(\tau) = \frac{8\beta}{3\alpha}\kappa_0^2\text{sech}^2(\kappa_0\tau),$$

with initial amplitude $a_0 = 8\beta\kappa_0^2/(3\alpha)$ and energy $E_0 = 256\beta^2\kappa_0^3/(27\alpha^2)$. In the presence of diffusion we use a perturbation theory for the soliton dynamics based on the inverse scattering transform, and we get that the initial soliton loses energy through the emission of continuous radiation. At leading order in μ , the soliton parameter evolves as [17]

$$(5.4) \quad \frac{d\kappa}{d\xi} = \frac{\mu\kappa^2}{8} \int \partial_\tau^2[\text{sech}^2(\kappa\tau)]\text{sech}^2(\kappa\tau)d\tau,$$

starting from $\kappa(0) = \kappa_0$. By computing the integral, we get the simple ODE $d\kappa/d\xi = -2\mu\kappa^3/15$. By integrating this equation, we find that the soliton amplitude and energy decay as

$$(5.5) \quad a(\xi) = \frac{a_0}{1 + \frac{4\xi}{15\xi_0}}, \quad E(\xi) = \frac{E_0}{\left(1 + \frac{4\xi}{15\xi_0}\right)^{3/2}},$$

where $\xi_0 = 1/(\mu\kappa_0^2)$. Note that $4/15 \simeq 0.27$. By comparing the amplitude decay rate of the soliton (5.5) with the one of the linear hyperbolic pulse (5.2), we observe that the soliton is initially more stable than the corresponding linear pulse. However, as the propagation distance increases, the soliton loses its stability and eventually becomes less stable than the linear pulse (see Figure 5.1). Indeed, the soliton stability results from a balance between dispersion and nonlinearity. Therefore, when the soliton amplitude decays, the nonlinear effects are reduced and it is natural to expect that the random and dispersive effects are no longer compensated for. The asymptotic decay rate of the soliton is $1/\xi$, while the asymptotic decay rate of the linear pulse is $1/\sqrt{\xi}$.

6. Numerical simulations. In this section we present numerical experiments that illustrate theoretical results obtained in this paper.

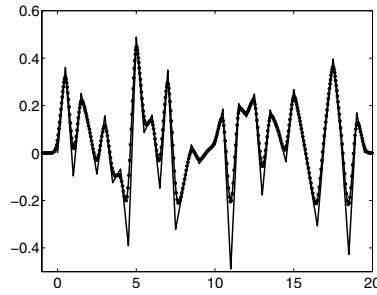


FIG. 6.1. The thin solid line plots a realization of the process n , and the thick dotted solid line is the corresponding realization of the process M . Here $l_c = 0.5$, $\sigma = 0.5$, $\beta = 0.25$.

6.1. Effective medium. Here we validate our probabilistic asymptotic analysis for the metric coefficient $M(\xi)$. This coefficient contains topographic information, and therefore our analysis is connected to an effective medium. We assume here that the random process n is continuous piecewise linear:

$$n(x) = \sum_j \mathbf{1}_{[jl_c, (j+1)l_c)}(x) (\eta_j + (\eta_{j+1} - \eta_j)(x/l_c - j)) ,$$

where the correlation length is l_c and $(\eta_j)_{j \geq 0}$ is a collection of independent and identically distributed random variables with uniform distribution over $(-\sigma, \sigma)$. As a result the effective diffusion coefficient is $\mu = \sigma^2 l_c / 6$ and

$$\hat{\gamma}(k) = \frac{4\sigma^2 l_c}{3} \frac{[1 - \cos(kl_c)]^2}{(kl_c)^4} .$$

In the first series of numerical experiments we have generated several realizations of the random process $n(x)$, and we have analyzed the statistical properties of the corresponding metric coefficient $M(\xi)$ (see Figure 6.1 for a realization). In particular in Figure 6.2 we compare the numerical average of M with the theoretical prediction (4.4) for the statistical mean of M , which here has the form

$$(6.1) \quad \mathbb{E}[M(\xi)] \simeq 1 - \frac{\sqrt{\beta}\sigma^2}{l_c} \frac{4 \ln 2}{3\pi} .$$

We consider different sets of values for the parameters l_c , σ , and β . It appears that the formula (6.1) for the theoretical mean is in good agreement with the numerical averages as long as l_c is not too small compared to $\sqrt{\beta}$, which is the regime for which the asymptotic theory is valid. In case (c), the expansion that leads to formula (6.1) is no longer valid; that is why a discrepancy can be observed. The Monte Carlo (Schwarz–Christoffel mapping) experiments for the metric term were done with the Schwarz–Christoffel Toolbox [8].

6.2. Effective wave behavior. Now we perform experiments in order to illustrate effective wave scattering properties. These other sets of numerical experiments have been performed to study wave propagation in different regimes. In these simulations we used $\sigma = 0.5$ and $l_c = 0.6$. First we present a Monte Carlo simulation illustrating the behavior predicted in Figure 5.1. Below we provide a physical interpretation for this figure. Then we consider the issue of the effective reduction of the

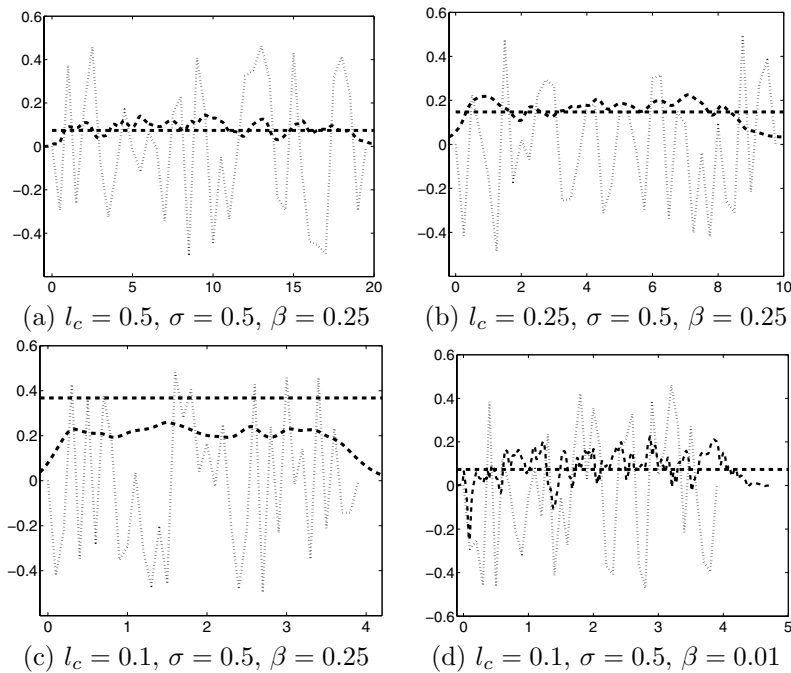


FIG. 6.2. Particular realizations of the process n are plotted in dotted lines. The straight lines represent the theoretical values (6.1). The dashed lines plot the averages of 60 realizations of the process M for (a) and (b) and 30 realizations for (c) and (d).

dispersion level, due to randomness, using the classical member of the Boussinesq family of systems (2.1)–(2.2), namely, for the relative depth value $y_0^2 = 1/3$. Over a flat bottom ($M \equiv 1$) this system reduces to the classical dimensionless (depth-averaged) Boussinesq system [29, 36].

For the first set of experiments we use a new spectral scheme developed for system (2.1)–(2.2), with $y_0^2 = 2/3$. This spectral scheme is specialized for this choice of y_0 . Details for this numerical scheme will be published elsewhere. The second set of numerical experiments was performed with the same predictor-corrector finite difference scheme as in [25, 26, 27]. Details can be found in these references. We chose to do this second set of experiments with $y_0^2 = 1/3$ for two reasons. First, we wanted to show that our observations are independent of the specific choice of y_0 . In this paper $y_0^2 = 2/3$ was chosen for technical reasons, so that the decoupling of equations was the most convenient for our analysis. Second, we chose $y_0^2 = 1/3$ because this value has the classical Boussinesq system as its underlying, flat bottom case. Moreover, this case had been extensively tested by the authors in [25, 26, 27, 11, 13] with a different numerical scheme. Hence we find it reassuring to test with both y_0 cases as well as with two different schemes.

On the one hand, we have performed numerical simulations with evanescent nonlinearity and dispersion $\alpha = \beta = 0$ and with an input sech^2 pulse with initial width $\kappa_0 = \sqrt{3}/2$. In this linear regime the theoretical decay for the pulse amplitude is given by (5.2) with $\xi_0 = 1/(\mu\kappa_0^2) = 53.3$. This theoretical formula can be compared directly with the results of the numerical simulations because the asymptotic analysis has shown that the variable ξ is equivalent to leading order to the propagation distance

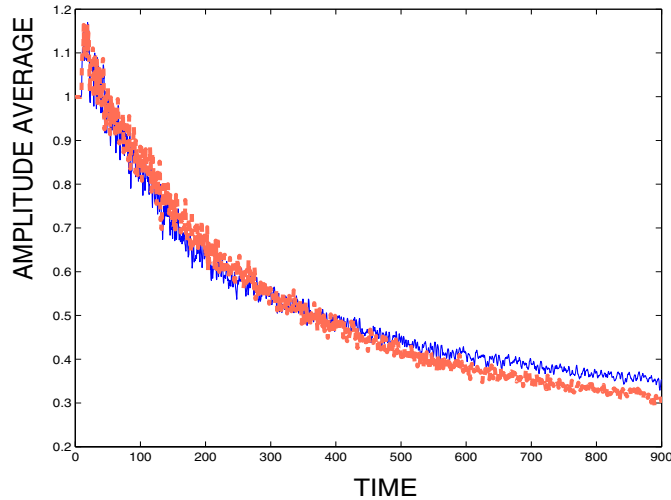


FIG. 6.3. The solid line corresponds to a linear nondispersive ($\alpha = \beta = 0$) wave, having a sech^2 profile, as the solitary wave. A total of 17 realizations for the bottom topography were used in computing the averaged amplitude decay for the wavefront. The dotted line corresponds to the solitary wave (namely, with $\alpha = \beta = 0.03$). A total of 19 realizations for the bottom topography were used in computing the corresponding averaged amplitude decay for the wavefront.

or to the propagation time (the velocity is normalized to one). On the other hand, we have carried out simulations in the nonlinear dispersive regime $\alpha = \beta = 0.03$, and we have considered an input sech^2 pulse with initial width $\kappa_0 = \sqrt{3}/2$ and amplitude corresponding to a soliton. The theoretical amplitude decay is then (5.5). Furthermore, the critical distance at which the soliton becomes less stable than the equivalent linear pulse is $4.2\xi_0 \simeq 225$. The results of the simulations are presented in Figure 6.3. The simulations have captured the amplitude decay of the sech^2 profile in both the linear hyperbolic and the solitary wave (namely weakly dispersive, weakly nonlinear) regimes. To reduce the residual fluctuations (since the parameter ε is not very small in the simulations) we perform several numerical experiments over different realizations of the bottom topography and average the amplitude over these realizations. The final result is presented in Figure 6.3, which matches very well with the theoretical result given in Figure 5.1.

An interesting physical interpretation can be given to the behavior described in Figure 5.1, obtained theoretically and illustrated numerically. We observe that after the soliton's amplitude has decayed beyond a certain threshold (and therefore the wave is in the linear dispersive regime) then it decays faster than its hyperbolic counterpart. A physical conclusion that one can extract from this fact is that monochromatic signals are converted faster into noise (i.e., into random fluctuations) than when travelling together with other Fourier modes. In other words, the linear hyperbolic sech^2 profile is more resistant to the random environment than its dispersive counterpart since all Fourier modes travel at the same phase speed. Once the solitary wave enters the linear regime (due to its amplitude decay) a nearly monochromatic oscillatory tail develops behind the wavefront [36], and this tail is more rapidly converted into noise.

Next we move on to our second set of experiments to provide a numerical illustration of the effective dispersion reduction due to the random environment. In

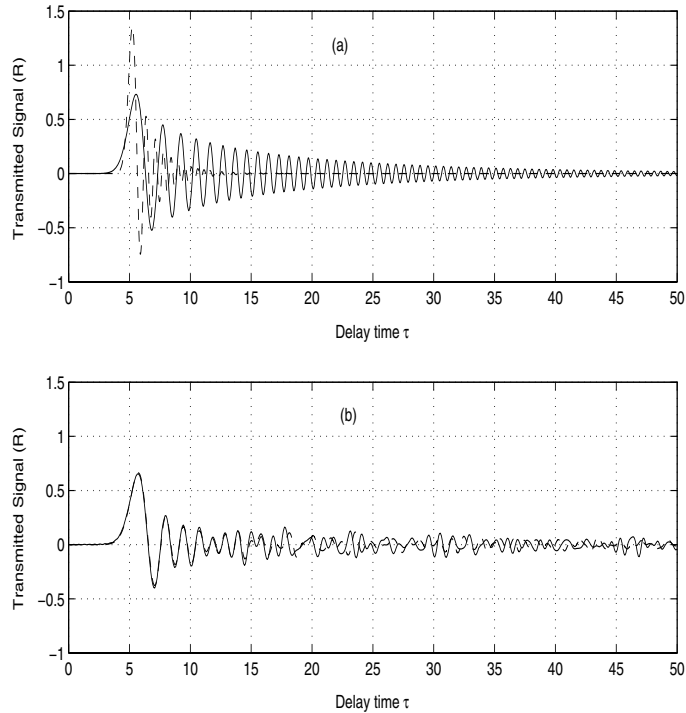


FIG. 6.4. *Reduction of the effective dispersion in the presence of randomness. The parameters are $\alpha = 0.001$ and $\beta = 0.01$. For the case of a flat bottom we have the top graph (a): An initial profile (dashed line) and a long time propagated pulse developing into an Airy function (solid line). For the case of a random topography (b): The solid line is the ODA approximation from [25], and the dashed line is the numerical solution of the Boussinesq system (with $y_0^2 = 1/3$). The leading deterministic pulse appears to be under less dispersion than the solution given in part (a), for a flat bottom, where the deterministic oscillatory tail is longer and decaying at a slower rate.*

Figure 6.4 we can see that the effective dispersion, due to the presence of randomness, is smaller than the original dispersion level of the model. A great part of the energy contained in the tail of the Airy function-type solution [25, 27] has been converted into a randomly fluctuating (transmitted and reflected) signal. In the linear regime, one mathematical manifestation of this phenomenon is through the ODA filter (namely a Gaussian kernel [11, 25]) that removes higher-frequency (short wave) components from the leading wavefront. Hence the wavefront has a smaller Fourier content, mostly of long wave modes, and hence appears to be under less dispersion. In Figure 6.4 this smaller effective dispersion is manifested by noting that the wavefront has a shorter deterministic oscillatory tail. This is equivalent to having an Airy kernel, say, in the solution of a linear KdV [11, 25], evaluated at an earlier time or with a smaller β . See (A.4) in [25].

But in this paper we are mostly concerned with the nonlinear regime. In Figures 6.5 and 6.6 we can see the same effect but now in the nonlinear regime. In these cases the effective decrease of dispersion is discussed in a different manner. In both examples, considering a flat bottom, a solitary wave is a travelling wave due to the perfect balance between dispersion and nonlinearity. In the presence of randomness the effective dispersion is smaller than that of the underlying model and hence smaller than the nonlinearity level. This lack of balance between the effective dispersion and

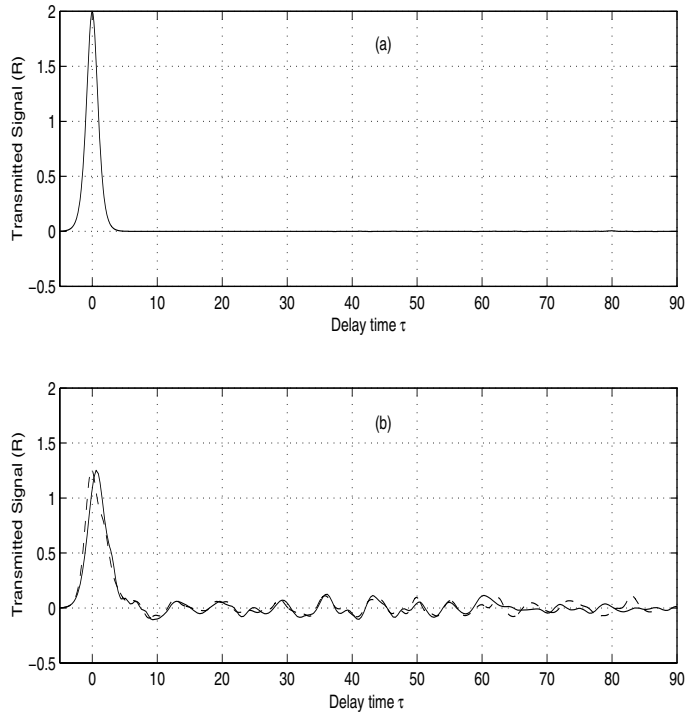


FIG. 6.5. The parameters are $\alpha = \beta = 0.005$. (a): The initial solitary wave together with a numerically propagated profile. After propagating over 25 pulse widths, no difference can be observed, and the numerical solution is, as expected, a travelling wave. Hence there is a perfect balance between nonlinearity and dispersion. (b): The profile predicted by the linear theory [25] (solid line) and the weakly nonlinear numerical experiment (dashed line). The regime is definitely not linear, and we observe the steepening at the wavefront due to the dispersion's effective reduction in the presence of randomness.

nonlinearity will produce a wavefront steepening. We will examine two levels of nonlinearity and see that the larger it is, the more intense is the steepening. In Figure 6.5 $\alpha = \beta = 0.005$ and the steepening is mild after the solitary wave has propagated over 25 times its effective pulse width. Note that the steepening is compared against the asymptotic result [25] for linear dispersive waves. In Figure 6.6 nonlinearity is stronger, by taking $\alpha = \beta = 0.01$, and this is clearly observed through the stronger steepening of the solitary wavefront. Thus the steepening along the solitary wavefront is a manifestation of a lack of balance between nonlinearity and dispersion, now effectively reduced by randomness as indicated by the theoretical results in this paper.

To summarize, we have shown computational experiments that illustrate the predictions of our asymptotic theory for the propagation medium, through the coefficient $M(\xi)$, and for dispersive long waves. In this paper the analysis was performed for a particular case of the terrain-following Boussinesq system, namely, with $y_0^2 = 2/3$. This was done for technical reasons. Hence numerical experiments were also performed for the case $y_0^2 = 1/3$, which relates to the classical (depth-averaged) Boussinesq system. Thus the effective behavior reported is not limited to a special choice of depth parameters. For a similar reason we chose to illustrate the theoretical results with two different numerical methods, one being specialized to the $y_0^2 = 2/3$ case.

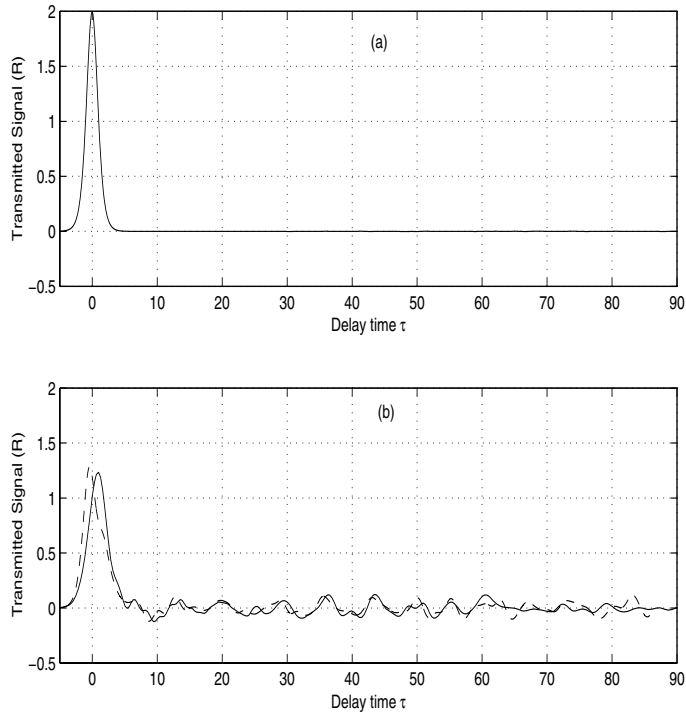


FIG. 6.6. The parameters are $\alpha = \beta = 0.01$. (a): The initial solitary wave together with a numerically propagated profile. After propagating over 25 pulse widths, no difference can be observed, and the numerical solution is, as expected, a travelling wave. (b): The profile predicted by the linear theory [25] (solid line) and the weakly nonlinear numerical experiment (dashed line). Now we observe even more steepening at the wavefront due to the dispersion's effective reduction in the presence of randomness and the fact that the nonlinearity parameter α is larger in this example.

REFERENCES

- [1] M. ASCH, W. KOHLER, G. PAPANICOLAOU, M. POSTEL, AND B. WHITE, *Frequency content of randomly scattered signals*, SIAM Rev., 33 (1991), pp. 519–625.
- [2] F. G. BASS, YU. S. KIVSHAR, V. V. KONOTOP, AND YU. A. SINITSYN, *Dynamics of solitons under random perturbations*, Phys. Rep., 157 (1988), pp. 63–181.
- [3] L. BERLYAND AND R. BURRIDGE, *The accuracy of the O'Doherty-Anstey approximation for wave propagating in highly disordered stratified media*, Wave Motion, 21 (1995), pp. 357–373.
- [4] N. N. BOGOLIUBOV AND Y. A. MITROPOLSKY, *Asymptotic Methods in the Theory of Non-Linear Oscillations*, Gordon and Breach, New York, 1961.
- [5] R. BURRIDGE, G. PAPANICOLAOU, AND B. WHITE, *One-dimensional wave propagation in a highly discontinuous medium*, Wave Motion, 10 (1988), pp. 19–44.
- [6] J.-F. CLOUET AND J.-P. FOUQUE, *Spreading of a pulse traveling in random media*, Ann. Appl. Probab., 4 (1994), pp. 1083–1097.
- [7] P. DEVILLARD, F. DUNLOP, AND B. SOUILLARD, *Localization of gravity waves on a channel with a random bottom*, J. Fluid Mech., 186 (1988), pp. 521–538.
- [8] T. DRISCOLL, *The Schwarz-Christoffel Toolbox for MATLAB*, <http://www.math.udel.edu/~driscoll/software/>.
- [9] D. V. EVANS, *The wide-spacing approximation applied to multiple scattering and sloshing problems*, J. Fluid Mech., 210 (1990), pp. 647–658.
- [10] D. V. EVANS AND C. M. LINTON, *On stepped approximations for water wave problems*, J. Fluid Mech., 278 (1994), pp. 229–249.
- [11] J.-P. FOUQUE, J. GARNIER, AND A. NACHBIN, *Time reversal for dispersive waves in random*

- media*, SIAM J. Appl. Math., 64 (2004), pp. 1810–1838.
- [12] J.-P. FOUQUE, J. GARNIER, AND A. NACHBIN, *Shock structure due to stochastic forcing and the time reversal of nonlinear waves*, Phys. D, 195 (2004), pp. 324–346.
- [13] J.-P. FOUQUE, J. GARNIER, J. C. MUÑOZ GRAJALES, AND A. NACHBIN, *Time reversing solitary waves*, Phys. Rev. Lett., 92 (2004), 094502.
- [14] J. GARNIER, *A multi-scaled diffusion-approximation theorem. Applications to wave propagation in random media*, ESAIM Probab. Statist., 1 (1997), pp. 183–206.
- [15] J. GARNIER AND A. NACHBIN, *The eddy viscosity for time reversing solitary waves in a dissipative environment*, Phys. Rev. Lett., 93 (2004), 154501.
- [16] J. GARNIER AND A. NACHBIN, *Eddy viscosity for gravity waves propagating over turbulent surfaces*, Phys. Fluids, 18 (2006), 055101.
- [17] V. I. KARPMAN, *Soliton evolution in the presence of perturbations*, Phys. Scripta, 20 (1979), pp. 462–478.
- [18] R. Z. KHASHMINSKII, *On stochastic processes defined by differential equations with a small parameter*, Theory Probab. Appl., 11 (1966), pp. 211–228.
- [19] H. J. KUSHNER, *Approximation and Weak Convergence Methods for Random Processes*, MIT Press, Cambridge, MA, 1984.
- [20] P. LEWICKI, *Long time evolution of wavefronts in random media*, SIAM J. Appl. Math., 54 (1994), pp. 907–934.
- [21] P. LEWICKI, R. BURRIDGE, AND G. PAPANICOLAOU, *Pulse stabilization in a strongly heterogeneous medium*, Wave Motion, 20 (1994), pp. 177–195.
- [22] C. C. MEI AND M. J. HANCOCK, *Weakly nonlinear surface waves over a random seabed*, J. Fluid Mech., 475 (2003), pp. 247–268.
- [23] C. C. MEI AND Y. LI, *Evolution of solitons over a randomly rough seabed*, Phys. Rev. E (3), 70 (2004), 016302.
- [24] D. MIDDLETON, *Introduction to Statistical Communication Theory*, McGraw–Hill, New York, 1960.
- [25] J. C. MUÑOZ GRAJALES AND A. NACHBIN, *Dispersive wave attenuation due to orographic forcing*, SIAM J. Appl. Math., 64 (2004), pp. 977–1001.
- [26] J. C. MUÑOZ GRAJALES AND A. NACHBIN, *Stiff microscale forcing and solitary wave refocusing*, Multiscale Model. Simul., 3 (2005), pp. 680–705.
- [27] J. C. MUÑOZ GRAJALES AND A. NACHBIN, *Improved Boussinesq-type equations for highly-variable depths*, IMA J. Appl. Math., 71 (2006), pp. 600–633.
- [28] A. NACHBIN, *The localization length of randomly scattered water waves*, J. Fluid Mech., 296 (1992), pp. 353–372.
- [29] A. NACHBIN, *A terrain-following Boussinesq system*, SIAM J. Appl. Math., 63 (2003), pp. 905–922.
- [30] A. NACHBIN AND G. PAPANICOLAOU, *Water waves in shallow channels of rapidly varying depth*, J. Fluid Mech., 241 (1992), pp. 311–332.
- [31] R. F. O'DOHERTY AND N. A. ANSTEY, *Reflections on amplitudes*, Geophys. Prospect., 19 (1971), pp. 430–458.
- [32] G. PAPANICOLAOU, *Asymptotic analysis of stochastic equations*, in Studies in Probability Theory, MAA Stud. Math. 18, M. Rosenblatt, ed., Mathematical Association of America, Washington, D.C., 1978, pp. 111–179.
- [33] G. PAPANICOLAOU, D. W. STROOCK, AND S. R. S. VARADHAN, *Martingale approach to some limit theorems*, in Statistical Mechanics and Dynamical Systems, D. Ruelle, ed., Duke Turbulence Conference, Duke Univ. Math. Series III, Part VI, Duke University, Durham, NC, 1976, pp. 1–120.
- [34] S. B. POPE, *Turbulent Flows*, Cambridge University Press, Cambridge, UK, 2000.
- [35] J. R. QUINTERO AND J. C. MUÑOZ GRAJALES, *Existence and uniqueness for a system of Boussinesq equations*, Methods Appl. Anal., 11 (2004), pp. 15–32.
- [36] G. B. WHITHAM, *Linear and Nonlinear Waves*, John Wiley, New York, 1974.